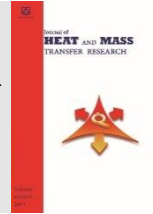




Semnan University



Research Article

Cooling of Two Hot Half-Cylinders through MHD Non-Newtonian Ferrofluid Free Convection under Heat Absorption; Investigation of Methods to Improve Thermal Performance via LBM

Mohammad Nemati ^{*,a}, Mohammad Sefid ^{†,a}, Arash Karimipour ^b

^a Faculty of Mechanical Engineering, Yazd University, Yazd, Iran

^b Department of Mechanical Engineering, Najafabad Branch, Islamic Azad University, Najafabad, Iran

PAPER INFO

Paper history:

Received: 2023-03-18

Revised: 2023-08-17

Accepted: 2023-08-19

Keywords:

Non-Newtonian ferrofluid free convection;
Heat absorption;
Entropy production;
Changing the hot objects position;
Changing the form of applied magnetic field;
Tilted right-triangular cavity.

ABSTRACT

The cooling process of parts in limited spaces is of great interest to researchers due to its many applications in industries such as electronics. Therefore, achieving the best performance of such systems has always been one of the challenges facing researchers. Due to this necessity, in the present simulation via the lattice Boltzmann method (LBM), the cooling of two hot semi-cylinders via magnetohydrodynamics (MHD) free convection has been interrogated. The novelty of the available study compared to antecedent studies is the effect of a magnetic field (MF) in different types and heat absorption for cooling two hot objects embedded within a triangular enclosure comprising non-Newtonian ferrofluid, which has not been studied so far. The accuracy of the obtained results was guaranteed via the validation of the written code in comparison with other studies qualitatively and quantitatively. Based on the results, To have a larger the Nusselt (Nu) value, at the highest Rayleigh (Ra) value, it is sufficient to decline the fluid power-law (PL) index, heat absorption index and the Hartmann (Ha) value. The reduction of in the mean Nu value due to rise of the Ha value for the shear thinning fluid is about 59%, while it is about 38% and 21% for the Newtonian and the shear thickening fluids, respectively. The existence of heat absorption, in addition to reducing the Nu value by about 75% in highest value, for the shear thinning fluid, results in a decrease in the value of thermal performance index (ITP), which is very insignificant for the shear thickening fluid at $Ha=60$. The predominance of conduction over convection is the result of enhancing the PL index, which diminishes the effect of type and power of MF . For $Ra=10^4$, due to low convection effects, changing the type of MF is ineffective, while for $Ra=10^6$, this effect is highest. By changing the angle of inclination of the chamber and changing the arrangement of hot objects on the walls of the cavity, by changing the flow patterns, the thermal characteristics of the system can be strongly affected. In all cases, the trend of the ITP changes is in accordance with the trend of the mean Nu changes, which exhibits that HT has the largest share to production entropy (PE).

DOI: [10.22075/jhmtr.2023.30230.1430](https://doi.org/10.22075/jhmtr.2023.30230.1430)

© 2023 Published by Semnan University Press. All rights reserved.

1. Introduction

The free convection heat transfer ($FCHT$) in regular or irregular closed cavities has many applications in

engineering and industry. Cooling systems of electronic equipment, heat insulation systems, nuclear reactors, as well as food storage industry are applications of enclosures in industry. In the $FCHT$, the

*Corresponding Author: Mohammad Nemati.

Email: mohammadnemati.lbm@gmail.com

†Corresponding Author: Mohammad Sefid.

Email: mhsefid@yazd.ac.ir

factor of creating flow is the difference in fluid density due to the difference in temperature of fluid layers in the presence of an acceleration field like the earth's gravity field [1-3]. It is possible to note the assumption of incompressibility, except for the buoyancy force generator, which is the same as the Boussinesq approximation [4-7]. The *FCHT* of Newtonian and non-Newtonian fluids in heated cavities is the reason for their importance and application in various types of fields such as cooling of nuclear reactors and components of electronic systems, food processing, polymer engineering has been investigated [8]. By using internal and external factors, this phenomenon can be controlled, among which this factors it can refer to applying a magnetic field (*MF*), adding metallic and non-metallic nanoparticles to the fluid performing the *FCHT*, influencing the radiation and heat absorption or heat production on the flow, and changing the geometric shape of the cavity. Among the studies related to this debate, it can remark the researches of Landl et al. [9], Bai et al. [10] and Zaim et al. [11]. Sheikholeslami [12]. addressed the modeling of the *FCHT* inside a porous chamber with a complex shape containing nanofluid in the presence of radiation using the control volume finite element method. The result of all these efforts revealed the enhancement of in buoyancy forces and heat transfer (*HT*) rate due to the increment of in the Rayleigh number (*Ra*).

Conventional fluids, which are used in many engineering processes and various industries, have always been considered to solve this defect due to their poor thermal performance. By dispersing non-metallic or metallic particles into this category of fluids, this defect is fixed, and thermal performance is improved. The *HT* properties of nanofluids depend on thermophysical properties of pure fluid and suspended nanoparticles, shape, size and percentage of nanoparticles [13-15]. The many advantages and applications of nanofluids have led many researchers to use this group of materials in their research [16]. By comparing the type of nanoparticles, Atashafrooz [17] reported that the use of copper oxide results in the higher *HT* compared to aluminum oxide. In addition, adding nanoparticles, regardless of their types, leads to the improvement of *HT*. Among other studies related to the use of nanofluids in enhancing *HT* rate and changing the flow characteristics, it can recourse to the study of Sheikholeslami [18] and Rajkumar et al. [19]. In daily life, industries and engineering processes, it is very common to encounter non-Newtonian fluids, including the cases where the non-Newtonian properties of fluids are used, such as the preparation of protective clothing to absorb bullet impact and, the preparation of molten polymers and atomic fluids [20-23]. In non-Newtonian fluid, unlike Newtonian fluid, viscosity does not have a constant value, and is strongly dependent on temperature and pressure [24].

In the most common type of non-Newtonian fluid flow modeling, the power-law (*PL*) fluid, apparent viscosity is important. In this sense, the viscosity is different at different points of the flow field, depending on the shear rate and the changes of different speeds in their direction. Based on the apparent viscosity, the non-Newtonian fluid with the *PL* model can be classified into two categories: the pseudoplastic and the dilatant. In the pseudoplastic fluid with high shear rates, the flow factor must prevail the lower shear stress compared to the Newtonian fluid. In the dilatant fluid with high shear rates, the flow factor must overcome the greater shear stress compared to Newtonian fluid [25-29]. Using the *PL* fluid, the evaluation of the *FCHT* inside a triangular chamber containing a cold barrier by Shah et al. [30]. The investigation of the *FCHT* inside a quarter-circle chamber containing a variable temperature barrier by Bai et al. [10] disclosed that by reducing the *PL* index (*PLI*) and the *Ra* increase, stronger currents are obtained, and *HT* rate increases. In addition, placing a barrier changes the flow and thermal characteristics in a certain way.

The effect of a *MF* on fluids that are electrically conductive is a very common issue in engineering processes, sometimes to reduce and sometimes to increase *HT* rate. In fact, this unwanted or wanted phenomenon can act as an unhelpful or helpful factor. Studying the effects of applied magnetic fields on magnetic fluids is vital to determine the changes in flow characteristics and *HT* [31-33]. It is very important how a *MF* is applied to the fluid current, because according to the buoyancy forces, the changes of these parameters create surprising effects. In some applications, simultaneously *MF* is coupled with heat absorption/generation. The tremendous impact of these two phenomena on the flow has been of great interest to scientists [34-39]. By simultaneously investigating the effect of *MF* at different angles and heat absorption/generation on nanofluid convection by Hussain et al [40], it was found that *HT* rate enhances with the increment of the heat absorption coefficient and the decrement of the Hartmann number (*Ha*). In addition to the diminish in temperature due to enhance in the percentage of nanoparticles, enhancing in *HT* rate was another finding.

The efficiency of a system can be calculated by calculating the irreversible production base on the second law of thermodynamics [41-43]. In this topic, many scholars have been conducted to evaluate the improvement of the thermal efficiency of *HT* equipment by calculating the production of entropy (*PE*), among which the research of Hajatzadeh et al. [44] can be hinted. They cleared that enhancing the *Ra* and the *Ha* have an enhancing and a decreasing impact on the rate of *HT* and irreversibility, respectively. In addition, the improvement of thermal performance was the result of increasing the percentage of

nanoparticles to the pure fluid. Iftikhar et al. [45] clarified the effect of variable *MF* on the nanofluid *FCHT*, within a square chamber containing a heat-generating blade. It was found that *PE* and *HT* rate decrease as the *Ha* increases. The reduction of the streamlines strength and the enhancement of the Bejan value due to the enhancement of *MF* strength are other results.

The issues that have been inspected as challenges during the study of this research are listed in the table 1. Interrogating methods to improve the cooling performance of two hot half-cylinders through the *FCHT* is the target of this numerical study by lattice Boltzmann method (*LBM*). According to prior studies (experimental and numerical) about thermal performance analysis of systems in which *HT* is important, several effective strategies have been proposed. Since the thermal performance analysis of non-Newtonian nanofluid in the desired geometry subjected to uniform/non-uniform *MF* and heat absorption has not been studied so far, the existing work has carefully addressed it.

Table 1. The effective strategies on thermal performance

1)	Varying the values of buoyancy forces
2)	Subjecting the nanofluid flow under influence of heat absorption and <i>MF</i> in different forms
3)	Varying the angle of chamber placement
4)	Varying the rheological behavioral of the pure fluid
5)	Subjecting the nanofluid flow under influence of heat absorption
6)	Varying the two hot semi-cylinders position

After reading this article, one can have a proper understanding of the change of the parameters mentioned in table 2 on the thermal characteristics of the system. Cooling two hot electronic components enclosed in a limited space is an example of the practical application of this research.

Table 2. The perused parameters along with the corresponding values

variable	range
1) The <i>Ha</i> value	$0 \leq Ha \leq 90$
2) The <i>Ra</i> value	$10^4 \leq Ra \leq 10^6$
3) The fluid behavioral index	$0.75 \leq n \leq 1.25$
4) The applied <i>MF</i> mode	MFM1, MFM2, MFM3
5) The angle of chamber placement	$0 \leq \lambda \leq 225^\circ$
6) The hot half-cylinders positions	Situation1, Situation2, Situation3
7) Heat absorption index	$-20 \leq Q \leq 0$

2. Simulation Definition

In order to cool the two hot half-cylinders through the free convection process, three different positions are considered according to Figure 1. Semi-cylinders with 0.125H diameter size are installed on the

horizontal and vertical adiabatic walls of the chamber. For the enclosure, the angle of rotation is described by λ index, according to which the position of the hot semi-cylinders is different with respect to the gravity force. Heat exchange takes place through the cold diagonal wall of the chamber. The right-triangular chamber is filled with non-Newtonian ferrofluid while inside the cavity there is uniform heat absorption with variable power as an effective internal factor. Horizontally from left to right, *MF* force is imposed on the current formed inside the chamber as an effective external factor. The range of the simulation variables is shown in Table 2.

3. Fluid Flow Governing Equations

The nanofluid modeling is based on the Table 3 [46-48]. The values related to the determining characteristics of nanofluids are revealed in Table 4 [49-51]. In this research, the effect of Brownian motion of particles has been observed, so a more accurate prediction of the effective properties of nanomaterials is expected. The Brownian motion is the omnidirectional and random movement of particles dispersed in the main fluid, which strongly affects the properties of nanofluid. This continuous movement of particles results in more dispersed particles [52-54].

Table 3. The governing equations in nanofluid relationships

$$\begin{aligned}
 (1) \quad & \rho_{NF} = \rho_{Fe_3O_4} \varphi_{Fe_3O_4} + \rho_{H_2O} (1 - \varphi_{Fe_3O_4}) \\
 (2) \quad & (\rho\beta)_{NF} = (\rho\beta)_{Fe_3O_4} \varphi_{Fe_3O_4} + (\rho\beta)_{H_2O} (1 - \varphi_{Fe_3O_4}) \\
 (3) \quad & (\rho C_p)_{NF} = (\rho C_p)_{Fe_3O_4} \varphi_{Fe_3O_4} + (\rho C_p)_{H_2O} (1 - \varphi_{Fe_3O_4}) \\
 & \mu_{Static} = \mu_{H_2O} (1 - \varphi_{Ag})^{-2.5} \\
 (4) \quad & \frac{\mu_{Brownian}}{5 \times 10^4 \beta^* \varphi_{Fe_3O_4} \rho_{H_2O}} = \sqrt{\frac{Tk_B}{(\rho d)_{Fe_3O_4}}} f(T, \varphi_{Fe_3O_4}) \\
 & \mu_{NF} = \mu_{Static} + \mu_{Brownian} \\
 (5) \quad & \sigma_{NF} = \sigma_{H_2O} \left[1 + \frac{3\varphi_{Fe_3O_4} \left(\frac{\sigma_{Fe_3O_4}}{\sigma_{H_2O}} - 1 \right)}{\left(\frac{\sigma_{Fe_3O_4}}{\sigma_{H_2O}} + 1 \right) - \varphi \left(\frac{\sigma_{Fe_3O_4}}{\sigma_{H_2O}} - 1 \right)} \right] \\
 & \frac{k_{Static}}{k_{H_2O}} = \frac{(k_{Fe_3O_4} + 2k_{H_2O}) - k_{Fe_3O_4} - 2\varphi_{Fe_3O_4} k_{H_2O}}{(k_{Fe_3O_4} + 2k_{H_2O}) + \varphi_{Fe_3O_4} (k_{H_2O} - k_{Fe_3O_4})} \\
 & \frac{k_{Brownian}}{5 \times 10^4 \beta^* \varphi_{Fe_3O_4} (\rho C_p)_{H_2O}} = \sqrt{\frac{Tk_B}{(\rho d)_{Fe_3O_4}}} f(T, \varphi_{Fe_3O_4}) \\
 (6) \quad & \left\{ \begin{aligned} & \beta^* = 0.0011(100\varphi_{Fe_3O_4})^{-0.7227} \\ & \text{for } \varphi \geq 0.01 ; k_B = 1.3807 \times 10^{-23} \\ & f(T, \varphi_{Fe_3O_4}) = [-6.04\varphi_{Fe_3O_4} + 0.4705] T \\ & + [1722.3\varphi_{Fe_3O_4} - 134.63] \\ & \text{for } 0.01 \leq \varphi \leq 0.04 \end{aligned} \right. \\
 & k_{NF} = k_{Static} + k_{Brownian} \\
 (7) \quad & \alpha_{NF} = \frac{k_{NF}}{(\rho C_p)_{NF}}
 \end{aligned}$$

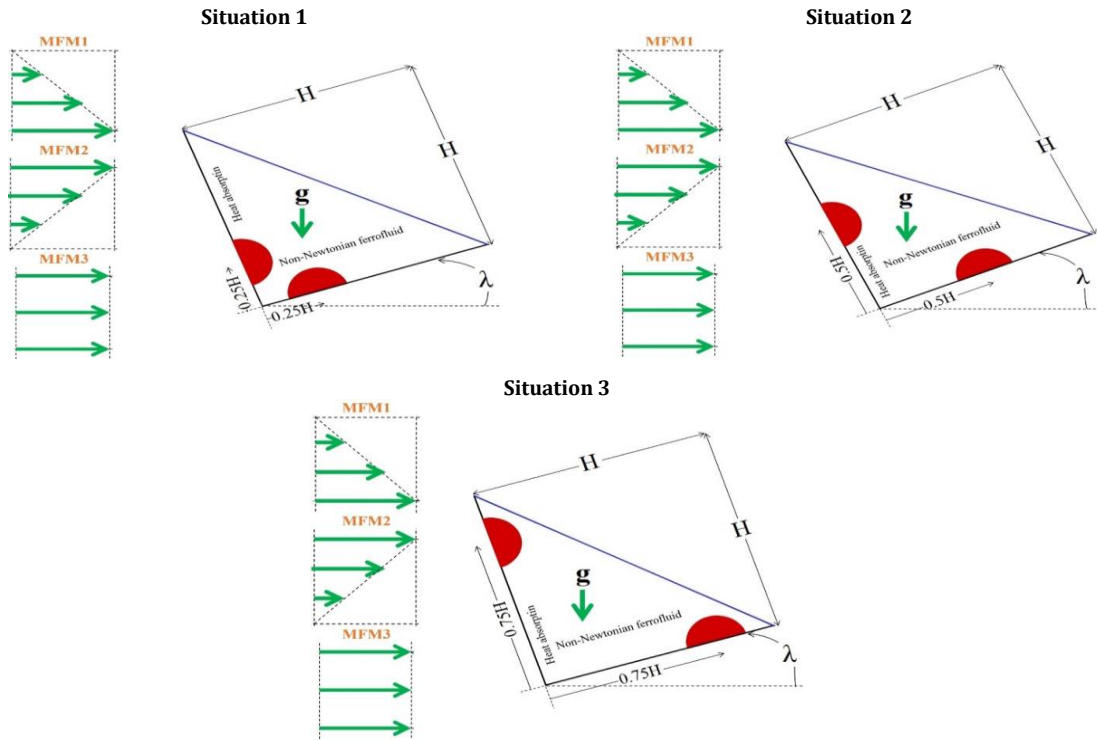


Figure 1. A schematic of the right-triangular cavity containing the two hot semi-cylinders

Table 4. The nanoparticles/pure fluid thermophysical properties [42]

property	Symbol	unit	Water (H2O)	Ferro particles (Fe ₃ O ₄)
The prandtl number	Pr	-	6.23	-
Electrical resistivity	σ	(kg ⁻¹ .m ⁻³ .s ³ .A ²)	0.05	25000
Thermal expansion	β	(K ⁻¹)	21×10 ⁻⁵	1.3×10 ⁻⁵
Heat capacity	C _p	(J.kg ⁻¹ .K ⁻¹)	4179	670
Thermal conductivity	k	(W.m ⁻¹ .K ⁻¹)	0.613	6
Density	ρ	(kg.m ⁻³)	997.1	5200

The parameter which considers different non-Newtonian fluid viscosities at each node in the simulation domain is estimated as mentioned in equations (1)-(3) [10, 55, 56]. *NF* in all the equations represent ferrofluid. The model equations governing flow movement are given in equations (4)-(7) [57-60]. The non-dimensional form of these equations are represented in equations (9)-(12) based on the non-dimensional parameters mentioned in equation (8). Defining stream function as per equation (13) helps in capturing the flow behavior of the considered fluid.

$$\tau_{ij} = \mu_{NF} \left(\frac{\partial u_i}{\partial x_j} + \frac{\partial u_j}{\partial x_i} \right) \quad (1)$$

$$\left\{ \begin{aligned} v(\mathbf{x}, t) &= v_0 |\gamma|^{(n-1)} \\ |\gamma| &= \sqrt{2 \times 0.5 \left(\frac{\partial u_i}{\partial x_j} + \frac{\partial u_j}{\partial x_i} \right) \times 0.5 \left(\frac{\partial u_i}{\partial x_j} + \frac{\partial u_j}{\partial x_i} \right)} \end{aligned} \right. \quad (2)$$

$$\mu_{H_2O} = \mu_0 \left\{ \left(\frac{\partial v}{\partial x} + \frac{\partial u}{\partial y} \right)^2 + 2 \left[\left(\frac{\partial u}{\partial x} \right)^2 + \left(\frac{\partial v}{\partial y} \right)^2 \right] \right\}^{\frac{(n-1)}{2}} \quad (3)$$

$$\frac{\partial u}{\partial x} + \frac{\partial v}{\partial y} = 0 \quad (4)$$

$$\rho_{NF} \left(u \frac{\partial u}{\partial x} + v \frac{\partial u}{\partial y} \right) = -\frac{\partial p}{\partial x} + \left(\frac{\partial \tau_{xx}}{\partial x} + \frac{\partial \tau_{xy}}{\partial y} \right) + \mathbf{g}(\rho\beta)_{NF} (T - T_{cold}) \sin \lambda \quad (5)$$

$$\rho_{NF} \left(u \frac{\partial v}{\partial x} + v \frac{\partial v}{\partial y} \right) = -\frac{\partial p}{\partial y} + \mathbf{g}(\rho\beta)_{NF} (T - T_{cold}) \cos \lambda + \left(\frac{\partial \tau_{xy}}{\partial x} + \frac{\partial \tau_{yy}}{\partial y} \right) - v B^2 \sigma_{NF} \quad (6)$$

$$u \frac{\partial T}{\partial x} + v \frac{\partial T}{\partial y} = \alpha_{NF} \left[\frac{\partial^2 T}{\partial x^2} + \frac{\partial^2 T}{\partial y^2} + \frac{\tilde{Q}}{(\rho C_p)_{NF}} \right] \quad (7)$$

The index that expresses the heat absorption of the system is displayed with \tilde{Q} . In the expressions mentioned above, *n* and *N* respectively indicate the fluid *PLI* and consistency parameter. The classification of *PL* fluid based on the *n* symbol is: the shear thinning or pseudoplastic fluid (*n*=0.75), the Newtonian fluid

($n=1$) and the shear thickening or dilatant fluid ($n=1.25$). For each considered parameter, the subscript zero represents the Newtonian fluid.

$$\begin{aligned} v_0 &= \frac{\mu_0}{\rho}, Pr = \frac{v_{H_2O}}{\alpha_{H_2O}}, \theta = \frac{T-T_c}{T_h-T_c}, Ha = BH^n \sqrt{\frac{\sigma \alpha^{1-n}}{\mu_0}}, \\ X &= \frac{x}{H}, Y = \frac{y}{H}, Ra = \frac{\beta_{H_2O} \theta g H^3}{v_{H_2O} \alpha_{H_2O}}, P = \frac{p H^2}{\rho Ra \alpha_{NF}^2}, \\ \alpha_{H_2O} &= \frac{v_{H_2O}}{Pr}, Q = \frac{\tilde{Q} H^2}{(\rho C_p)_{H_2O} \alpha_{H_2O}}, \\ U &= \frac{u H}{\alpha_{H_2O} \sqrt{Ra}}, V = \frac{v H}{\alpha_{H_2O} \sqrt{Ra}} \end{aligned} \tag{8}$$

$$\frac{\partial U}{\partial X} + \frac{\partial V}{\partial Y} = 0 \tag{9}$$

$$\begin{aligned} U \frac{\partial U}{\partial X} + V \frac{\partial U}{\partial Y} &= -\frac{\partial P}{\partial X} + \frac{(\rho \beta)_{NF}}{\rho_{NF} \beta_{H_2O}} Pr \theta \sin \lambda \\ &+ \frac{Pr(\rho_{H_2O}) [2 \frac{\partial}{\partial X} (\frac{\mu_{H_2O}}{N} \frac{\partial U}{\partial X}) + \frac{\partial}{\partial Y} (\frac{\mu_{H_2O}}{N} \frac{\partial U}{\partial Y} + \frac{\partial V}{\partial X})]}{\sqrt{Ra} [\rho_{NF} (1 - \phi_{Fe_3O_4})]^{2.5}} \end{aligned} \tag{10}$$

$$\begin{aligned} U \frac{\partial V}{\partial X} + V \frac{\partial V}{\partial Y} &= -\frac{\partial P}{\partial Y} + \frac{(\rho \beta)_{NF}}{\rho_{NF} \beta_{H_2O}} Pr \theta \cos \lambda \\ &+ \frac{Pr(\rho_{H_2O}) [2 \frac{\partial}{\partial Y} (\frac{\mu_{H_2O}}{N} \frac{\partial V}{\partial Y}) + \frac{\partial}{\partial X} (\frac{\mu_{H_2O}}{N} \frac{\partial U}{\partial X} + \frac{\partial V}{\partial Y})]}{\sqrt{Ra} [\rho_{NF} (1 - \phi_{Fe_3O_4})]^{2.5}} \end{aligned} \tag{11}$$

$$\begin{aligned} \frac{\rho_{H_2O}}{\rho_{NF}} \frac{Pr Ha^2}{\sqrt{Ra}} \frac{1}{(1 - \phi_{Fe_3O_4})^{2.5}} \frac{\sigma_{NF}}{\sigma_{H_2O}} V \\ U \frac{\partial \theta}{\partial X} + V \frac{\partial \theta}{\partial Y} = \frac{\alpha_{NF}}{\alpha_{H_2O}} \frac{1}{\sqrt{Ra}} [(\frac{\partial^2 \theta}{\partial X^2} + \frac{\partial^2 \theta}{\partial Y^2}) + Q \theta] \end{aligned} \tag{12}$$

$$U = \frac{\partial \Psi}{\partial Y} \text{ and } V = -\frac{\partial \Psi}{\partial X} \tag{13}$$

The dimensional and non-dimensional form of *PE* expressions for entropy estimation are given in equations (14) and (15), respectively [61-63]. The subscripts 1, 2 and 3 in these relations correspond to *PE* due to fluid friction, *HT* and *MF*, respectively. Also, (\sim) superscript correspond to dimensional equations. The total *PE* given by equation (16) is estimated as the sum of main production factors.

The average Nusselt value (*Nu*) on cold wall is calculated in equation (17) to estimate the *HT* rate. In analyzing the thermal efficiency of the system, a parameter called thermal performance index (*ITP*) is used, which is defined according to equation (18). This index expresses the ratio of the mean *Nu* value to the total *PE*.

The important criteria considered for the computation is given in equation (19) in which the number of iterations is denoted by superscript *b*.

Following cases are the assumptions made to model the aforementioned problem:

- All flow boundaries are impermeable, and there is no slip on the surfaces.
- Incompressible is considered as the investigated flow regime.
- Simulations have been performed for laminar, steady, and 2D flow.
- Inclusion of density variation is taken through the Boussinesq approximation.
- Uniform spherical nano-sized particles have been used.
- There is a thermal equilibrium between nanoparticles and base fluid particles.
- Viscous dissipation as well as radiation *HT* is neglected.

$$\tilde{S} = \tilde{S}_1 + \tilde{S}_2 + \tilde{S}_3 :$$

$$\left\{ \begin{aligned} \tilde{S}_1 &= \frac{\mu_{NF}}{T_H + T_C} [2((\frac{\partial u}{\partial x})^2 + (\frac{\partial v}{\partial y})^2) + (\frac{\partial u}{\partial y} + \frac{\partial v}{\partial x})^2] \\ \tilde{S}_2 &= \frac{k_{NF}}{(T_H + T_C)^2} [(\frac{\partial T}{\partial x})^2 + (\frac{\partial T}{\partial y})^2] \\ \tilde{S}_3 &= \frac{B^2 \sigma_{NF}}{T_H + T_C} V^2 \end{aligned} \right. \tag{14}$$

$$S = S_1 + S_2 + S_3 :$$

$$\left\{ \begin{aligned} S_1 &= \chi \frac{\mu_{NF}}{\mu_{H_2O}} [2((\frac{\partial U}{\partial X})^2 + (\frac{\partial V}{\partial Y})^2) + (\frac{\partial U}{\partial Y} + \frac{\partial V}{\partial X})^2] \\ S_2 &= \frac{k_{NF}}{k_{H_2O}} [(\frac{\partial \theta}{\partial X})^2 + (\frac{\partial \theta}{\partial Y})^2] \\ S_3 &= \chi \frac{\sigma_{NF}}{\sigma_{H_2O}} Ha^2 V^2 \\ \chi &= \frac{\mu_{H_2O}}{k_{H_2O}} \frac{T_H + T_C}{2} (\frac{V}{T_H - T_C})^2 \end{aligned} \right. \tag{15}$$

$$S = \int_0^1 \int_0^1 S \, dX dY = \int_0^1 \int_0^1 [S_1 + S_2 + S_3] \, dX dY \tag{16}$$

$$\left\{ \begin{aligned} Nu &= \frac{1}{H} \int_0^1 \frac{k_{NF}}{k_{H_2O}} (\frac{\partial \theta}{\partial n}) \, dn \\ n &: \text{Perpendicular to the surface} \end{aligned} \right. \tag{17}$$

$$ITP = \frac{Nu}{S} \tag{18}$$

$$\left| \frac{Nu^{b+1} - Nu^b}{Nu^b} \right| \leq 10^{-5} \tag{19}$$

4. LBM Formulation

Equation (20) describes the Boltzmann equation used in *LBM* obtained by discretizing time as well as space [64-66]. f_i and f_i^{eq} indicate density and equilibrium distribution functions, respectively, and c_i is based on the chosen model. D^*Q^{**} denotes the model utilized for discretization of the Boltzmann

equation on grid. Here, * and ** respectively denote the dimensional and number of lines allowed for particle movement. For flow as well as thermal field, D₂Q₉ model is used. Figure 2 (a) displays an example of this model in computational domain. Equations (21)-(22) provides c_i value along with the equilibrium distribution function of the flow field. Equation (23) which describes the relation between kinematic viscosity and flow field relaxation time (τ_1) is used in order to get Navier-Stokes equation from Boltzmann equation [67-69]. Equations (24) and (25) solves the lattice Boltzmann equation in collision as well as streaming stages. In these equations, the distribution function after the stage of collision is denoted by \tilde{f}_i . Buoyancy as well as magnetic force terms appear in equation (26) which denote the external forces considered in the present investigation [67-69]. Calculation of kinematic viscosity through shear rate via LBM is based on equation (27) [69]. The Boltzmann equation which ignores the consideration of viscous dissipation is provided in equation (28) for energy field [56-58]. Equation (29) is used to describe the equilibrium distribution function which corresponds to the thermal field (h^{eq}). Also, for correct recovery of energy equation from lattice Boltzmann thermal equation, equation (30) is considered in terms of thermal diffusion coefficient [2].

$$f_i(\mathbf{x}+\mathbf{c}_i,t+1)=f_i(\mathbf{x},t)+\frac{[f_i^{eq}(\mathbf{x},t)-(f_i(\mathbf{x},t))]}{\tau_1(\mathbf{x},t)} \quad (20)$$

$$\mathbf{c}_i = \begin{pmatrix} c_{ix} \\ c_{iy} \end{pmatrix} = \begin{pmatrix} 0 & 1 & 0 & -1 & 0 & 1 & -1 & -1 & 1 \\ 0 & 0 & 1 & 0 & -1 & 1 & 1 & -1 & -1 \end{pmatrix} \quad (21)$$

$$f_i^{eq} = \omega_i [1 + 3(\mathbf{c}_i \cdot \mathbf{u}) - \frac{9}{2}(\mathbf{u} \cdot \mathbf{u}) + \frac{3}{2}(\mathbf{c}_i \cdot \mathbf{u})^2] \quad (22)$$

$$\tau_1(\mathbf{x},t) = 3\nu(\mathbf{x},t) + 0.5 \quad (23)$$

$$\tilde{f}_i(\mathbf{x}+\mathbf{c}_i,t+1) = \tilde{f}_i(\mathbf{x},t) + \frac{[f_i^{eq}(\mathbf{x},t) - (f_i(\mathbf{x},t))]}{\tau_1(\mathbf{x},t)} \quad (24)$$

$$f_i(\mathbf{x}+\mathbf{c}_i,t+1) = \tilde{f}_i(\mathbf{x},t+1) \quad (25)$$

$$f_i(\mathbf{x}+\mathbf{c}_i,t+1) = f_i(\mathbf{x},t) + \frac{[f_i^{eq}(\mathbf{x},t) - (f_i(\mathbf{x},t))]}{\tau_1(\mathbf{x},t)} + 3\mathbf{c}_i \cdot [-\nu\omega_i\rho_{H_2O}Ha^2(\frac{\mu_{NF}}{H^2}) + \omega_i\mathbf{g}(\rho\beta)_{NF}\theta] \quad (26)$$

$$\tau_1(\mathbf{x},t) = 3\nu(\mathbf{x},t) + 0.5, \quad \nu(\mathbf{x},t) = \frac{Pr}{(\sqrt{Ra})^{(2-n)}} |\gamma|^{(n-1)}, \quad (27)$$

$$\gamma_{ij} = -\frac{3}{2\rho c^2 \tau_1(\mathbf{x},t)} \sum_{i=0}^8 c_{ix} c_{iy} (f_i - f_i^{eq})$$

$$h_i(\mathbf{x}+\mathbf{c}_i,t+1) = h_i(\mathbf{x},t) + \frac{[h_i^{eq}(\mathbf{x},t) - h_i(\mathbf{x},t)]}{\tau_2(\mathbf{x},t)} + \frac{\tilde{Q}}{(\rho C_p)_{NF}} (T - T_C) \quad (28)$$

$$h_i^{eq} = \omega_i T [1 + 3(\mathbf{c}_i \cdot \mathbf{u})] \quad (29)$$

$$\tau_2(\mathbf{x},t) = 3\alpha(\mathbf{x},t) + 0.5 \quad (30)$$

Furthermore, equations (31) and (32) represent the weighting factor concerning D₂Q₉ lattice arrangement along with the macroscopic values [16, 29, 35]. τ_2 in the above equation corresponds to thermal field relaxation time.

$$\omega_0 = \frac{4}{9}, \omega_{1-4} = \frac{1}{9}, \omega_{5-8} = \frac{1}{36} \quad (31)$$

$$\rho = \sum_{i=0}^8 f_i, \mathbf{u} = \frac{\sum_{i=0}^8 \mathbf{c}_i f_i}{\rho}, T = \sum_{i=0}^8 h_i \quad (32)$$

In the computational study, for the sake of accuracy and convergence speed, a suitable algorithm is essential. For finding the solution of the governing equations by LBM, Table (5) displays the solution process, which is used as an algorithm in the present study.

Table 5. An algorithm to solve the problem by LBM

Step 1	Determination of initial values
Step 2	Calculation of the distribution functions
Step 3	Implementation of the collision stage
Step 4	Implementation of the streaming stage
Step 5	Calculation of the macroscopic quantity such as density and speed
Step 6	Applying boundary conditions
Step 7	Calculation of the shear rate in the domain nodes

Notice: The solution is obtained if the obtained results are converging after 7th step based on the considered convergence criterion. Otherwise, the repeat the calculations from 2nd step.

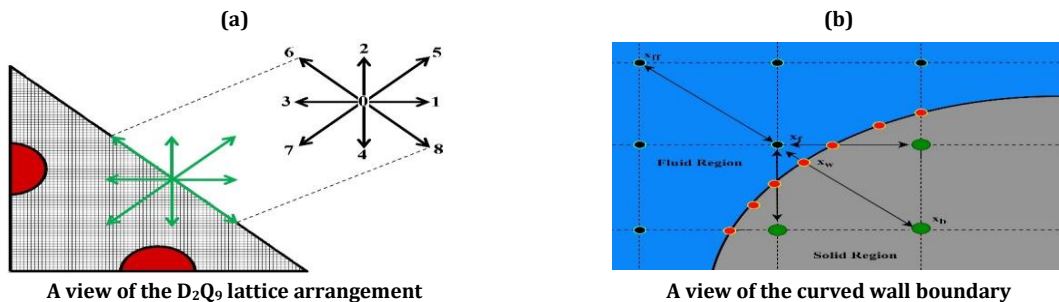


Figure 2. The lattice arrangement in boundaries

To exert the conditions of boundary on the smooth and diagonal walls, the bounce back model according to references [67-69] was used. In this model, the unknown distribution functions entered into the domain are designated based on the known distribution functions out of the computational scope. The boundary conditions on the cavity walls are in accordance with equations (33)-(35) due to Figure 2 (a).

Diagonal wall

$$\left\{ \begin{array}{l} \text{Velocity boundary conditions :} \\ \left\{ \begin{array}{l} f(4,i,j)=f(2,i,j) \\ f(7,i,j)=f(5,i,j) \\ f(3,i,j)=f(1,i,j) \end{array} \right. \\ \text{Temperature boundary conditions :} \\ \left\{ \begin{array}{l} h(4,i,j)=h(2,i,j) \\ h(7,i,j)=h(5,i,j) \\ h(3,i,j)=h(1,i,j) \end{array} \right. \end{array} \right. \quad (33)$$

Horizontal wall

$$\left\{ \begin{array}{l} \text{Velocity boundary conditions :} \\ \left\{ \begin{array}{l} f(2,i,0)=f(4,i,0) \\ f(5,i,0)=f(7,i,0) \\ f(6,i,0)=f(8,i,0) \end{array} \right. \\ \text{Temperature boundary conditions :} \\ \left\{ \begin{array}{l} h(2,i,0)=h(4,i,0) \\ h(5,i,0)=h(7,i,0) \\ h(6,i,0)=h(8,i,0) \end{array} \right. \end{array} \right. \quad (34)$$

Vertical wall

$$\left\{ \begin{array}{l} \text{Velocity boundary conditions :} \\ \left\{ \begin{array}{l} f(1,0,j)=f(3,0,j) \\ f(5,0,j)=f(7,0,j) \\ f(8,0,j)=f(6,0,j) \end{array} \right. \\ \text{Temperature boundary conditions :} \\ \left\{ \begin{array}{l} h(1,0,j)=h(3,0,j) \\ h(5,0,j)=h(7,0,j) \\ h(8,0,j)=h(6,0,j) \end{array} \right. \end{array} \right. \quad (35)$$

Due to the definition of LBM in the cartesian grid, modeling the curved boundary in this method has always been associated with complications. The bounce back model, despite its simplicity, has a lot of error, especially at high the *Ra* values, that is why other methods have been proposed [70]. Filippova and Hänel [71] presented the first boundary condition model with second-order accuracy in order to simulate the curved boundary. This method is actually based on the definition of a kind of virtual distribution function for the nodes near the border of the curve. In this method, according to Figure 2 (b), based on the location of the boundary node *w* between two nodes *b* and *f*, the variable Δ_{curved} is defined as $\Delta_{\text{curved}} = \frac{x_f - x_w}{x_f - x_b}$ [72].

Subscript *w*: indicator of the intersection of the curved boundary with the Cartesian lattice, subscript *b*: the nodes in the solid region, and subscripts *f* and *ff*: the first and second nodes in each of the directions of the grid within the computational domain. The virtual distribution function for point *b* in \vec{a} direction (perpendicular of curved surface), based on linear interpolation, is calculated regarding to equations (36) and (37) [73]. As suggested by Shahriari et al. [58], equations (38) is used to calculate χ and \vec{u}_{bf} . In above equations, $\vec{c}_a = -\vec{c}_a$. To apply the temperature boundary conditions accurately, the method recommended by Wang et al. [59] is used. The two parameters \vec{u}_b^* and T_b^* are determined according to equations (42)-(47) depending on the Δ_{curved} value [60].

$$\tilde{f}_a(\vec{x}_b, t) = (1 - \chi)\tilde{f}_a(\vec{x}_f, t) + \chi f_a^*(\vec{x}_b, t) - \frac{3}{c^2} 2\rho\omega_a(\vec{x}_f, t)\vec{c}_a \cdot \vec{u}_w \quad (36)$$

$$f_a^*(\vec{x}_b, t) = f_a^{\text{eq}}(\vec{x}_f, t) + \rho\omega_a(\vec{x}_f, t) \frac{3}{c^2} \vec{c}_a \cdot (\vec{u}_{bf} - \vec{u}_f) \quad (37)$$

$$\left\{ \begin{array}{l} \text{if } 0 \leq \Delta_{\text{curved}} < 0.5 \rightarrow \\ \vec{u}_{bf} = \vec{u}_{ff} = \vec{u}(\vec{x}_{ff}, t), \chi = \frac{2\Delta_{\text{curved}} - 1}{(3\nu + 0.5) - 1} \\ \text{if } 0.5 \leq \Delta_{\text{curved}} \leq 1 \rightarrow \\ \vec{u}_{bf} = \vec{u}_f + \frac{3}{2\Delta_{\text{curved}}} (\vec{u}_w - \vec{u}_f), \chi = \frac{2\Delta_{\text{curved}} - 1}{(3\nu + 0.5) - 0.5} \end{array} \right. \quad (38)$$

$$\tilde{h}_a(\vec{x}_b, t) = \tilde{h}_a^{\text{eq}}(\vec{x}_b, t) + (1 - \frac{1}{(3\alpha + 0.5)}) h_a^{\text{neq}}(\vec{x}_b, t) \quad (39)$$

$$h_a^{\text{eq}}(\vec{x}_b, t) = \omega_a T_b^* (\vec{x}_b, t) [1 + \frac{3}{c^2} (\vec{c}_a \cdot \vec{u}_b^*)] \quad (40)$$

$$h_a^{\text{neq}}(\vec{x}_b, t) = \Delta_{\text{curved}} h_a^{\text{neq}}(\vec{x}_f, t) (1 - \Delta_{\text{curved}}) h_a^{\text{neq}}(\vec{x}_{ff}, t) \quad (41)$$

$$\left\{ \begin{array}{l} \text{if } \Delta_{\text{curved}} > 0.75 \rightarrow \vec{u}_b^* = \vec{u}_{b1} \\ \text{if } \Delta_{\text{curved}} \leq 0.75 \rightarrow \vec{u}_b^* = \vec{u}_{b1} + (1 - \Delta_{\text{curved}}) \vec{u}_{b2} \end{array} \right. \quad (42)$$

$$\left\{ \begin{array}{l} \text{if } \Delta_{\text{curved}} > 0.75 \rightarrow T_b^* = T_{b1} \\ \text{if } \Delta_{\text{curved}} \leq 0.75 \rightarrow T_b^* = T_{b1} + (1 - \Delta_{\text{curved}}) T_{b2} \end{array} \right. \quad (43)$$

$$\vec{u}_{b1} = \frac{1}{\Delta_{\text{curved}}} [\vec{u}_w + (\Delta_{\text{curved}} - 1) \vec{u}_f] \quad (44)$$

$$\vec{u}_{b2} = \frac{1}{(1 + \Delta_{\text{curved}})} [2\vec{u}_w + (\Delta_{\text{curved}} - 1) \vec{u}_{ff}] \quad (45)$$

$$T_{b1} = \frac{1}{\Delta_{\text{curved}}} [T_w (\Delta_{\text{curved}} - 1) T_f] \quad (46)$$

$$T_{b2} = \frac{1}{(1 + \Delta_{\text{curved}})} [2T_w (\Delta_{\text{curved}} - 1) T_{ff}] \quad (47)$$

5. Checking the Solution Sensitivity

Table 6 displays the difference in the mean *Nu* for various lattice sizes. These values are estimated for *Ha*=30 and *Ha*=90. To attain the desired accuracy, the outcomes obtained in current study are examined, and it is found that after a particular lattice size, the values of the mean *Nu* value are independent of the lattice

points for $Ra=10^6$, $Q=0$, $\varphi=0.04$, $\lambda=0$, and MFM3 at situation 1. Considering this independence of the solution, an optimal grid size of 121×121 is chosen to perform further calculations in the current simulation.

For validating the available work, verification between present results with that of the previous studies is obligatory. In this computational analysis, we have considered qualitative as well as quantitative validation cases which are represented in Figure 3 and Figure 4, respectively. The effect of MF on isotherms and entropy lines on the PL fluid free convection in $n=0.75$ for the present simulation and the study of Bai et al. [10] are compared in Figure 4. This figure provides a qualitative validation of present work. In Figure 4 (a), the present work is compared quantitatively with the study of Bai et al. [10] from the point of view of PE for changes of the Ha value and the

PL criterion at semi hot barrier mode for $Ra=10^5$ and the uniform horizontal MF .

In addition to this, another quantitative comparison have been displayed in Figure 4 (b). This figure provides a clear visualization of comparison of the mean Nu value between the available work and the study of Afsana et al. [39] for different values of the PLI and the Ha values in $Ra=10^5$. This comparison was done for magnetohydrodynamics (MHD) free convection in a sinusoidally heated chamber. As seen from Figure 3 and Figure 4, a quite good agreement in qualitative and quantitative aspect is observed between this study and the results of references. Due to the low deviation between the obtained results, the accuracy and precise performance of the study findings can be guaranteed.

Table 6. Inquiring the sensitivity of the mean Nu value to the change of network sizes $\text{Difference} = \left| \frac{Nu^{\text{Next lattice size}} - Nu^{\text{Previous lattice size}}}{Nu^{\text{Previous lattice size}}} \right| (\%)$

	61×61	91×91	121×121	151×151	181×181
Ha=0					
n=0.75	8.911	9.153	9.295	9.401	9.497
Difference	-	2.72	1.55	1.15	1.02
n=1.25	2.953	3.016	3.051	3.079	3.102
Difference	-	2.13	1.16	0.92	0.75
Ha=90					
n=0.75	3.648	3.752	3.815	3.861	3.903
Difference	-	2.85	1.68	1.21	1.09
n=1.25	2.023	2.069	2.095	2.119	2.139
Difference	-	2.27	1.25	1.15	0.95

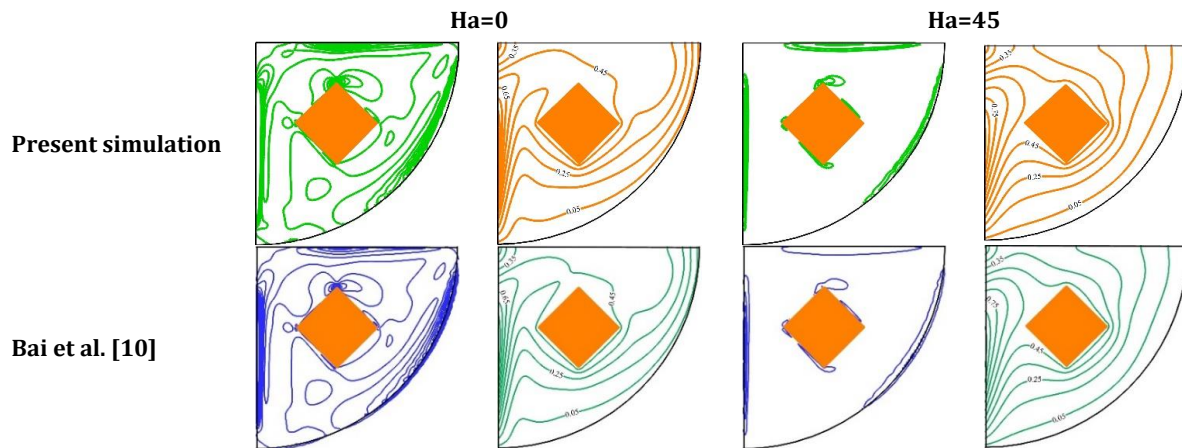


Figure 3. The qualitatively comparison results between the present work and Bai et al. [10]

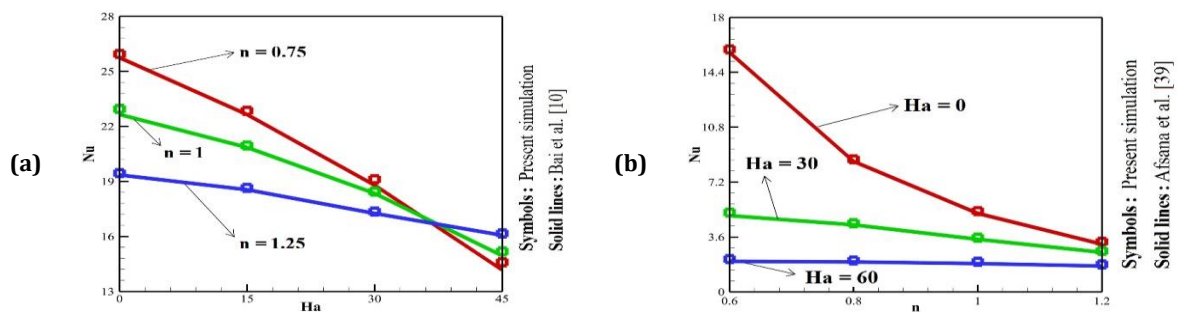


Figure 4. The quantitatively comparison results between the present work and references

6. Results

Isotherms and entropy lines due to fluid friction are presented in Figure 5. Four points can be deduced:

- 1- The result of enhancing the Ha value is increasing the strength of the Lorentz force. Considering that the MF is applied perpendicular to the gravitational force and from left to right

(pay attention to Figure 1), the Lorentz force is imposed on the fluid flow against the buoyant forces (pay attention to equations (6) and (26)). This factor leads to the reduction of thermal convection characteristics, and its manifestation can be seen in the reduction of the density of isotherms in the near of the cold wall and the less curved density lines near the hot objects.

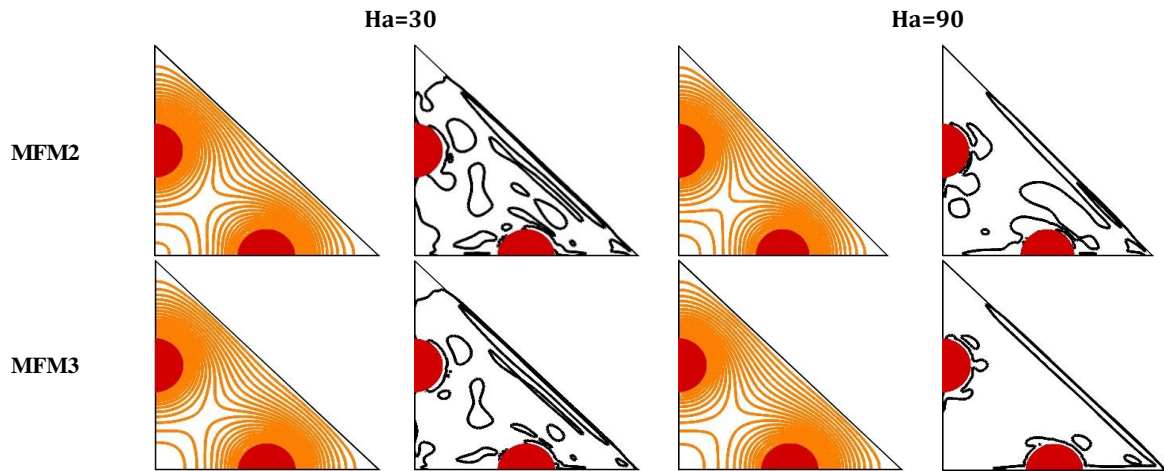


Figure 5 (a). Flow patterns at $Ra=10^4$ due to variation of the Ha value and form of applied MF

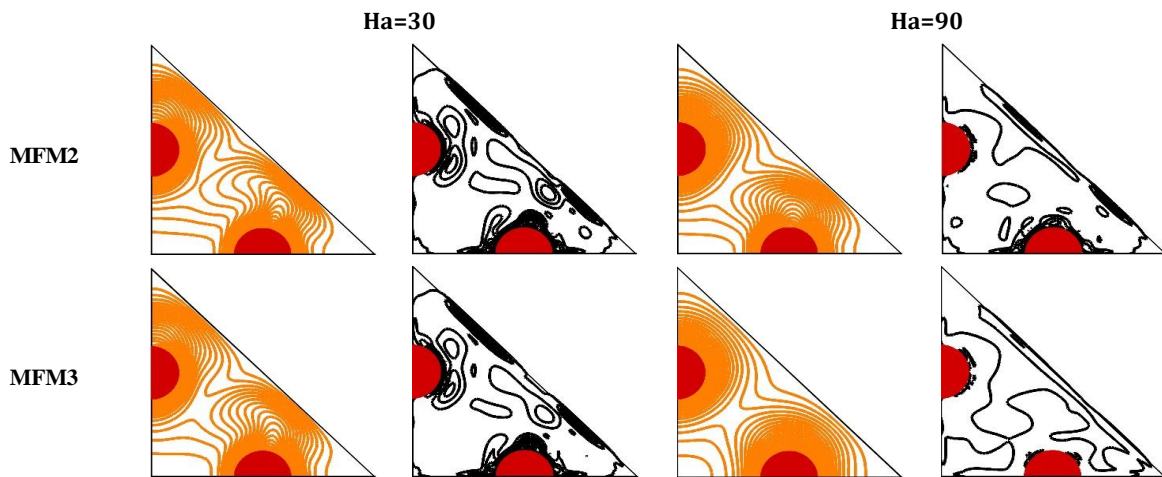


Figure 5 (b). Flow patterns at $Ra=10^5$ due to variation of the Ha value and form of applied MF

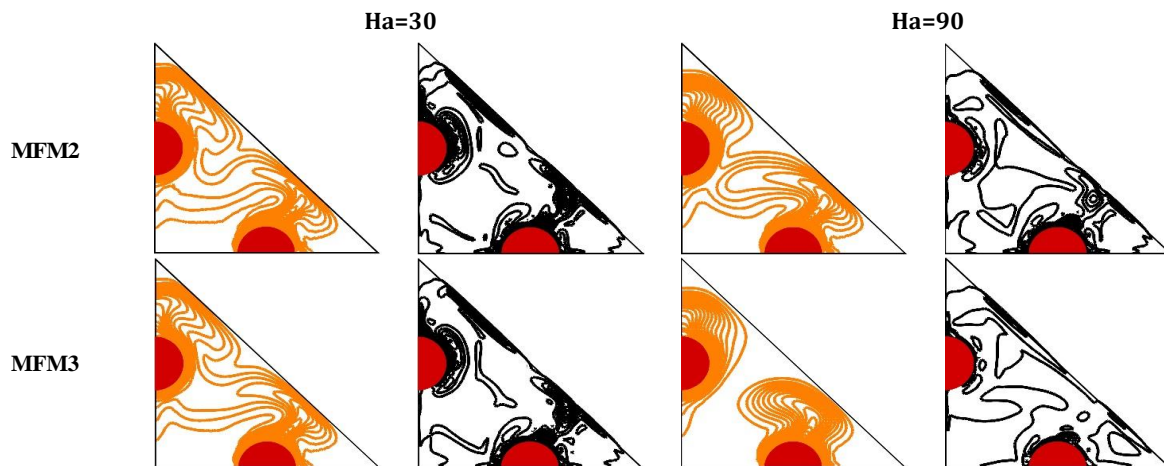


Figure 5 (c). Flow patterns at $Ra=10^6$ due to variation of the Ha value and form of applied MF

- 2- Since the strength of buoyancy forces enhances with the enhancing the Ra value, the fluid rotates with greater power inside the chamber and this factor leads to an increase in disturbances and curvatures of isotherms. Absence of isotherm curvature and placement of lines parallel to the walls in $Ra=10^4$ illustrates the HT at the molecular level (the dominance of heat conduction over convection). Due to the low power of thermal convection in $Ra=10^4$, enhancing the Ha value is meaningless and ineffective considering the flow patterns.
- 3- The change in the form of the applied MF in both cases (non-uniformly or uniform) changes the characteristics of the flow. Considering that by applying the MF in the form of MFM2, less Lorentz force is imposed on the current compared to MFM3, the effects of the imposed MF are less. However, the important point is that the change in the exerted MF is more noticeable for enhancing the Ha value and the Ra value.
- 4- According to equations (14)-(16), the decrease in the concentration of entropy lines is justified by the reduction of the Ra value and the Ha value. Because in these situations, the low convection power leads to the reduction of temperature and speed gradients (the main factors to production of entropy).

The decrement of in horizontal velocity due to the enhancing in the Ha value and the decreasing in Ra value is clearly illustrated in Figure 6. The reason for the greater effect of the applied MF for enhancement of the Ra value can be deduced in the greater effect of convection power. To reduce the effect of exerted MF , it is requisite to apply this external field as MFM2. Because in this mode, the greatest amount of this resistive force enters the flow in the upper part of the chamber. As the amount of MF force is applied from the lower part of the chamber, the decrease in speed and the gradients related to speed and flow are more apparent. However, the least influence in changing MF type on the flow is related to $Ra=10^4$.

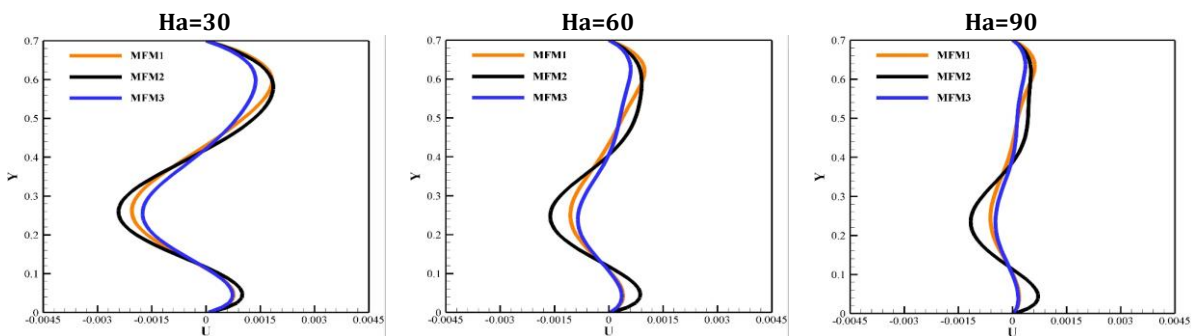


Figure 6 (a). Horizontal velocity at $Ra=10^4$ due to variation of the applied MF and the Ha value

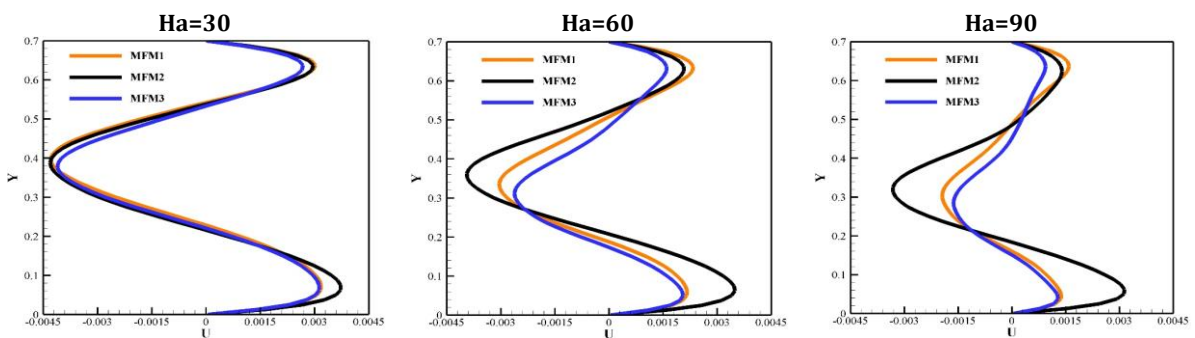


Figure 6 (b). Horizontal velocity at $Ra=10^5$ due to variation of the applied MF and the Ha value

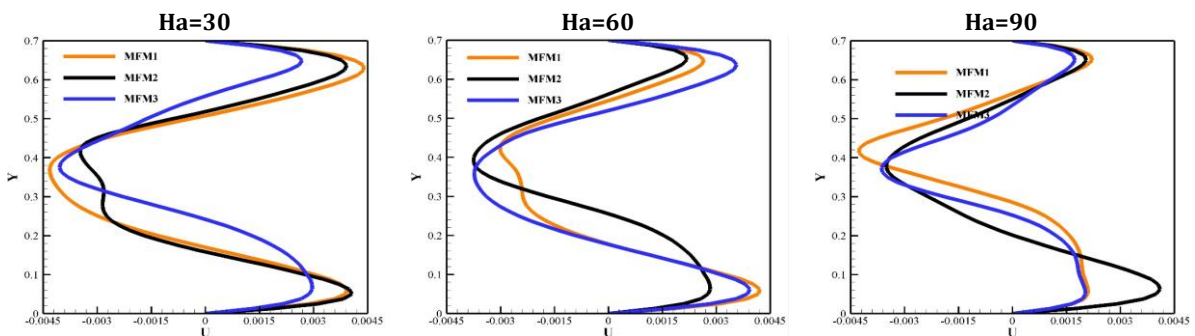


Figure 6 (c). Horizontal velocity at $Ra=10^6$ due to variation of the applied MF and the Ha value

According to the content presented about Figure 5 and Figure 6, it was predictable that the average Nu value would decrease as the Ha value enhances. According to Figure 7, it is almost ineffectual to change the type of MF and increase the Ha value for $Ra=10^4$. The lowest effect of the Ha value increase in high the Ra values belongs to MFM2, and the highest effect is related to MFM3. Quantitatively, for $Ra=10^5$, for enhancing the Ha value from 0-90, the mean Nu value diminishes by 52%, 44%, and 59%, respectively for MFM1, MFM2, and MFM3, and this effect for $Ra=10^6$ is around 40%, 32% and 68%, respectively. The changes in the graphs in terms of different variables are similar to the average Nu value for the thermal performance index in Figure 7. The decrease in the ITP value due to the increase in the Ha value indicates that the ratio of the decrease in the mean Nu value is greater than the decrease in the entropy value. The highest ITP value belongs to $Ra=10^6$ in the absence of the MF , which is about 35% and 60% higher than $Ra=10^5$ and $Ra=10^4$, respectively.

By simultaneously changing the arrangement of hot parts on the adiabatic walls and the angle of the chamber placement, special and different thermal characteristics can be achieved, as seen in Figure 8. According to Figure 8 (a), for situation 1, there is pure thermal conduction for the chamber placed in $\lambda=225^\circ$. Where the isotherms are completely parallel to the diagonal wall, and isotherms are concentrated around the hot body. Because according to Rayleigh-Bernard's

theory, in a situation where the cold wall is placed at the bottom, and the heat source is placed at the top, the free convection process is severely disrupted, and there is the weakest performance. For $\lambda=180^\circ$, the situation is a little better, but still the situation is the same as for $\lambda=225^\circ$. By changing the arrangement of the hot bodies, the conditions will be slightly improved, and the distortion of the isotherms near the cold wall leads to better heat exchange. The thermal conditions for and are far better than the other two angles. In addition to observing the symmetry of the lines for the angles of 45° and 225° according to the cavity placement angle, it can be seen that for situation 2, there is the greatest expansion and distortion of the isotherms within the triangular enclosure. Due to this issue, situation 2 is the best mode in terms of convection process. Because in this case, the hot objects are located between the cold wall and the adiabatic walls.

In Figure 8 (b), in addition to the symmetry of the entropy lines for and , the negligible of the formed entropy for situation 1 in and is very evident. For angles of 0 and 45 degrees, the higher entropy formed due to fluid friction is justified due to the higher convection power for these angles. Especially in where the cold wall is above the heat source, and the best performance is there in terms of convection. Therefore, by changing the position of hot components, the entropy value and the average Nu value can be managed.

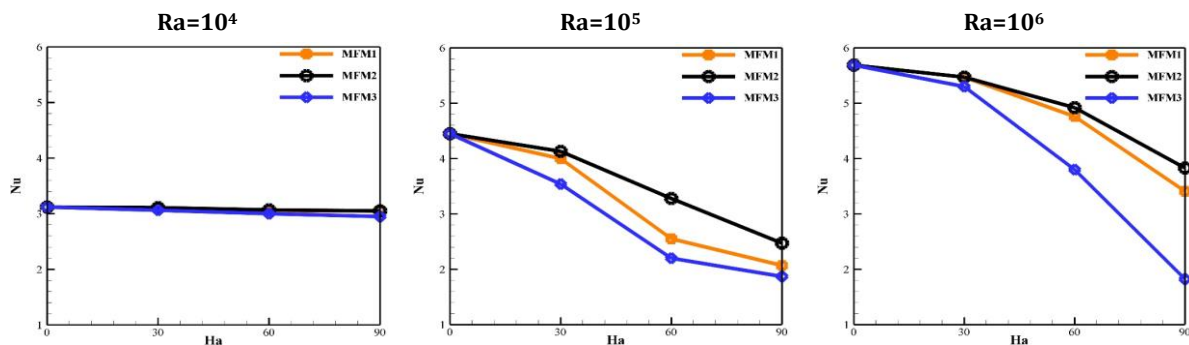


Figure 7 (a). The values of mean Nu value due to variation of the Ra value, the type of applied MF and the Ha value

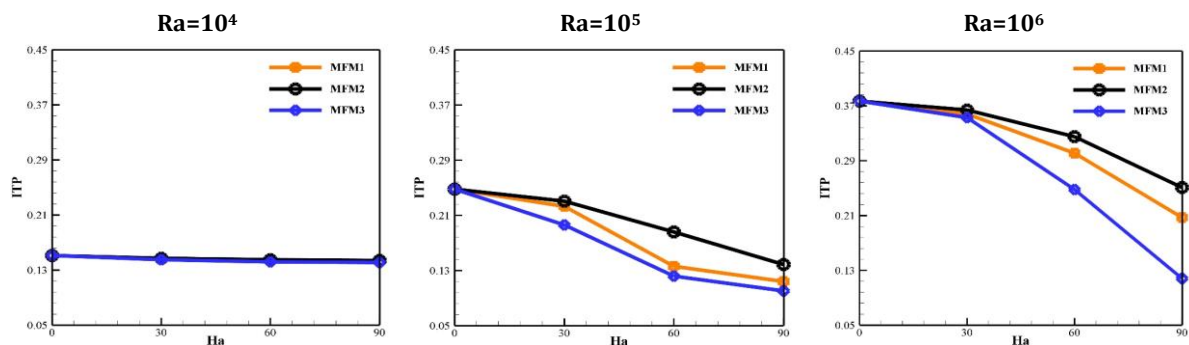


Figure 7 (b). The values of the ITP due to variation of the Ra value, the type of applied MF and the Ha value

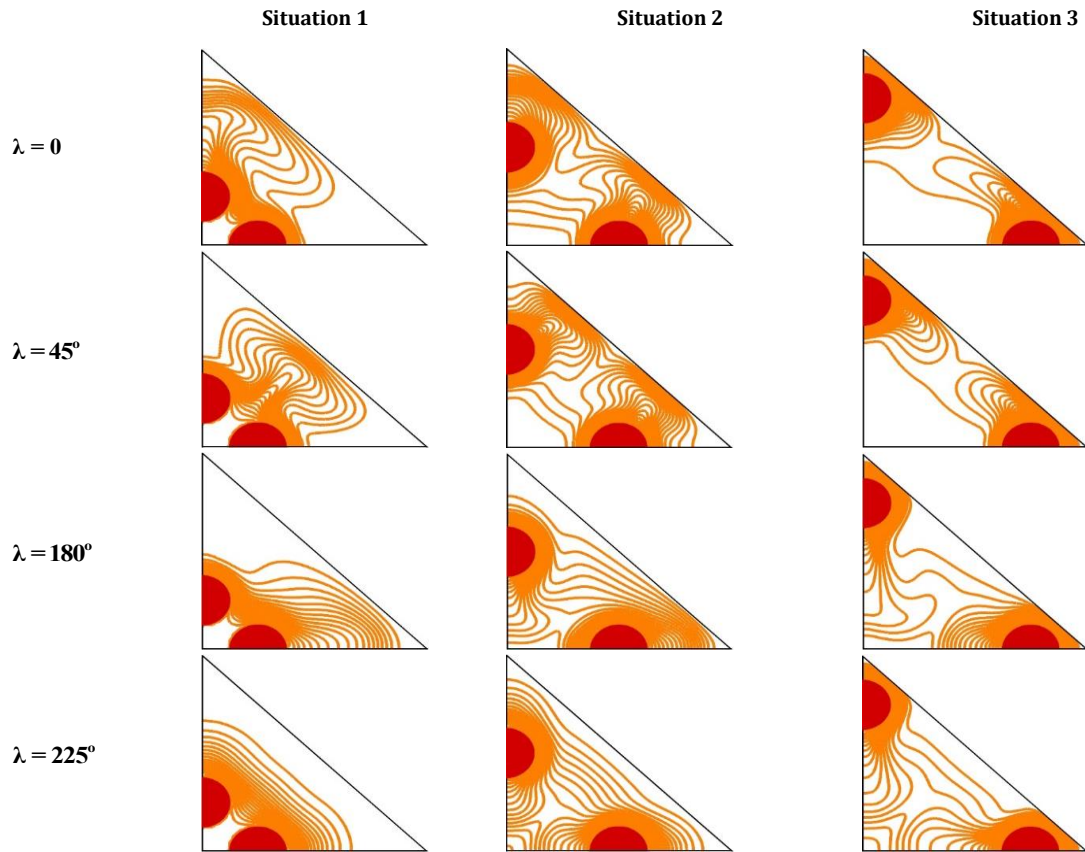


Figure 8 (a). Isotherms due to variation of the chamber placement angle and the position of arrangement of hot bodies at $Ra=10^5$

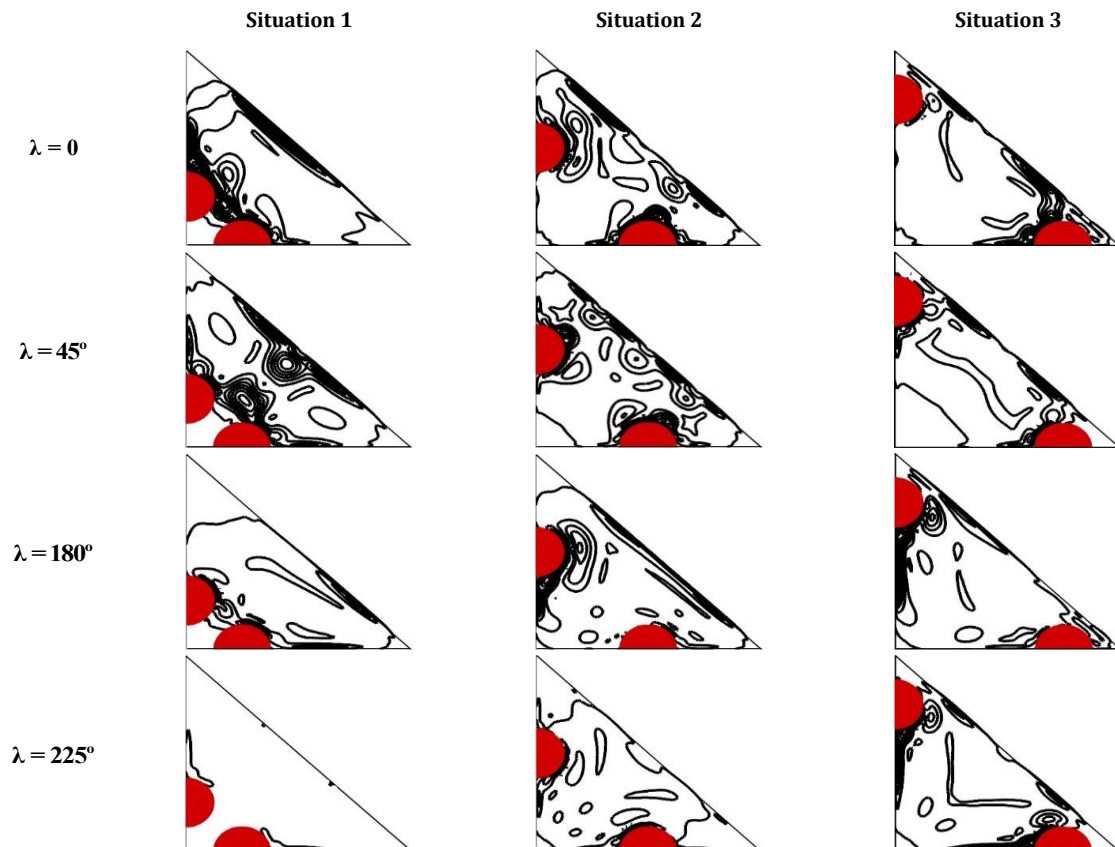


Figure 8 (b). Entropy lines due to variation of the chamber placement angle and the position of arrangement of hot bodies at $Ra=10^5$

According to Figure 9, for all situations, the highest average Nu value is acquired when the chamber is placed at $\lambda=45^\circ$. As explained for Figure 8, since the dense isotherms were on the hot bodies in $\lambda=180^\circ$ and $\lambda=225^\circ$, it is not far-fetched that the lowest mean Nu value belongs to these angles. The important point is that the difference of the average Nu values for different angles is very small for situation 1. In all three situations, for $\lambda=180^\circ$ and $\lambda=225^\circ$, applying or not applying the MF is the same. Because the strength of the buoyancy forces in these two angles is very low, and the MF cannot affect the thermal characteristics. However, for the situation 2 for $\lambda=0$ and $\lambda=45^\circ$, according to the slope of the graphs, the further reduction of the mean Nu value for the increase of the Ha value attracts attention (according to the explanations described in Figure 8 (a)). The trend of the ITP variations slightly different from the mean Nu value is reported in Figure 9. For situation 1, where there are minimal convection effects, the ITP variations for different the Ha values are very small, however, the highest coefficient of performance belongs to $\lambda=45^\circ$. The important point is the slight difference in the ITP values in situation 1. In situation 2 and situation 3, for enhancing the Ha value, a decrease in the ITP value for $\lambda=0$ and $\lambda=45^\circ$ is observed. However, for $\lambda=225^\circ$ in situation 2 and situation 3, an increase in ITP can be achieved. For $\lambda=180^\circ$, it is possible to reduce the ITP

for situation 2 and increase for situation 3. The difference of the isotherms contours for the change of the PLI becomes more noticeable as the strength of the buoyancy force increases.

According to Figure 10, for $n=0.75$, because the fluid moves with lower viscosity, it has more ability to rotate more strongly inside the chamber. Because according to equations (1)-(3), with the enhancement of the n parameter, the viscosity of the fluid enhances. The greater isotherms scattering is a sign of enhancing convection power for reducing the n parameter. For $n=0.125$ isotherms are dense around hot bodies. The remarkable point is that there is no significant change in the isotherms for the change of the n parameter according to $Ra=10^4$. Because in this mode, the buoyancy power is low, whether the fluid has low viscosity or high viscosity, it does not have the ability to rotate strongly. The appearance of the impact of heat absorption on the isotherms patterns is such that the concentration of the lines in the near of the cold wall is reduced and the lines are concentrated around the hot objects which this effect becomes more distinct for the Ra value reduction. For $Ra=10^4$ in all values of the PLI and in all values of the Ha values and at $Ra=10^5$ and $Ra=10^6$ for some states, condensation isotherm is not observed on the cold wall, which indicates poor cooling performance.

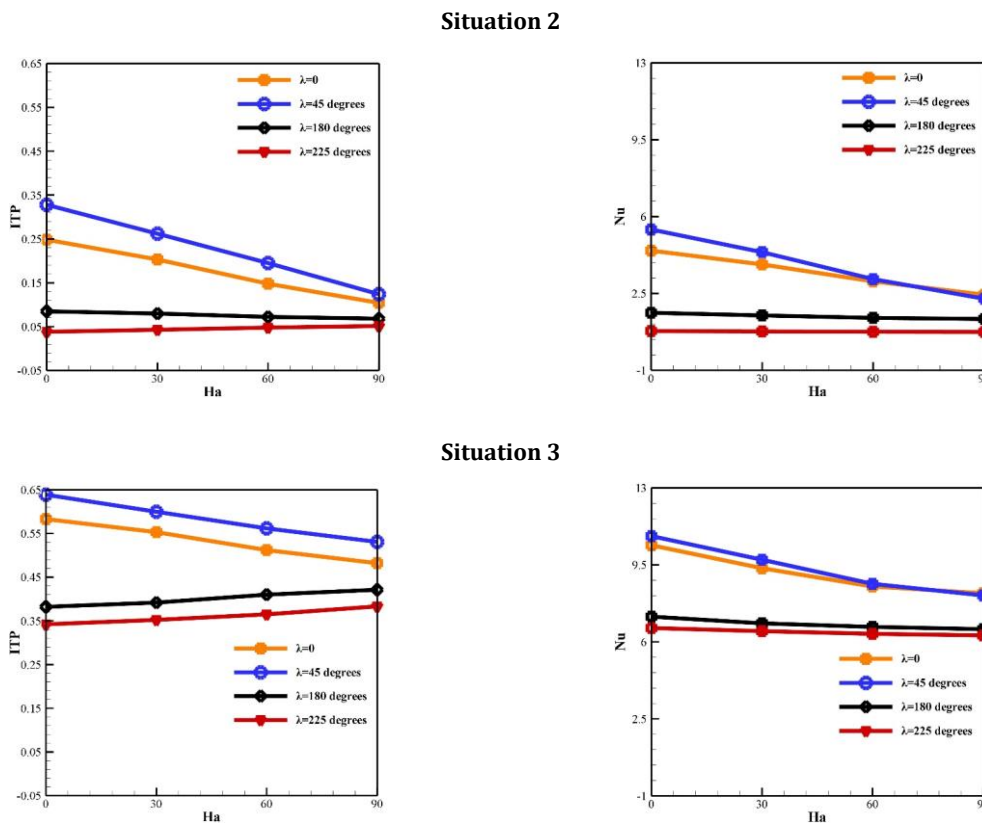


Figure 9. The values of mean Nu and the ITP due to variation of configuration type, chamber inclination angle and the Ha value

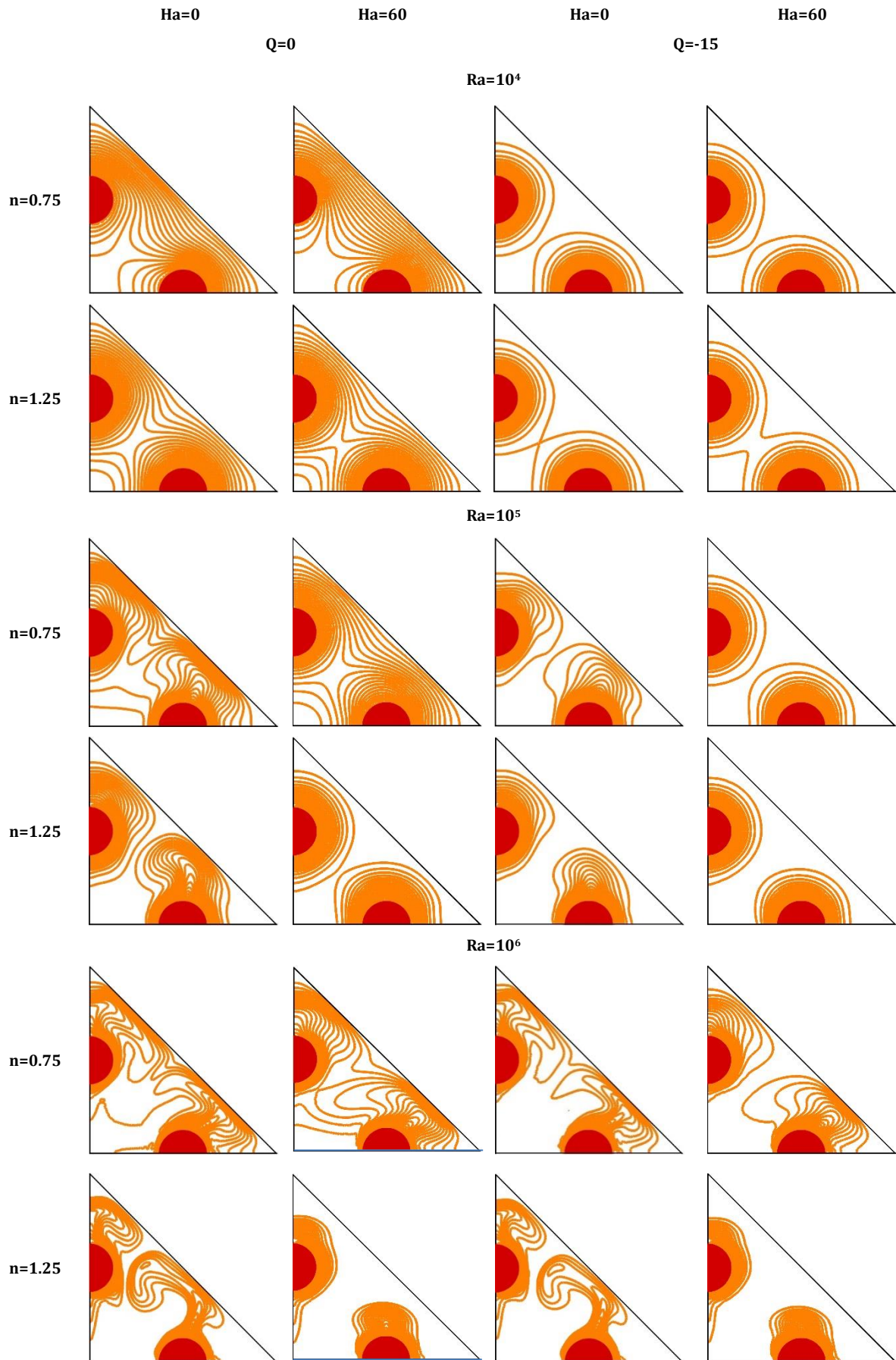


Figure 10. Isotherms due to variation of the Ha value, the Ra value, the PLI value and heat absorption coefficient

In addition to the declines in the speed value due to the increase in the *MF* strength, the decrease in the fluid flow speed due to the increase in the *PLI* is quite evident. For $n=1$ and $n=1.25$, enhancing the *Ha* value to more than 60 is ineffective. To reduce the effect of *MF* on the flow speed, one of the proposed ways is to increase the fluid viscosity, as can be observed in Figure 11.

Changes in the average *Nu* value for enhancing the *Ha* value have a decreasing trend for all values of the *PLI* and heat absorption coefficient based on Figure 12(a). In all values of the *PLI*, the lowest mean *Nu* value is related to the highest value of heat absorption parameter in terms of quantity, as explained in Figure

10. With the enhancement of the *PLI*, the difference between the graphs decreases, so the effectiveness of heat absorption for the shear thickening fluid is reported to be the lowest. According to the prediction and analysis of the results in Figure 10, the trend of the *ITP* changes is similar to the mean *Nu* value based on Figure 12(b). Quantitatively, as the value of the heat absorption coefficient enhances, the percentage of reduction in the mean *Nu* value is much higher than the entropy decrease due to the increase of the heat absorption coefficient. Although enhancing the heat absorption coefficient leads to decrease in entropy formation due to the limited heat difference, but the percentage of this decrease is not enough to improve the thermal performance.

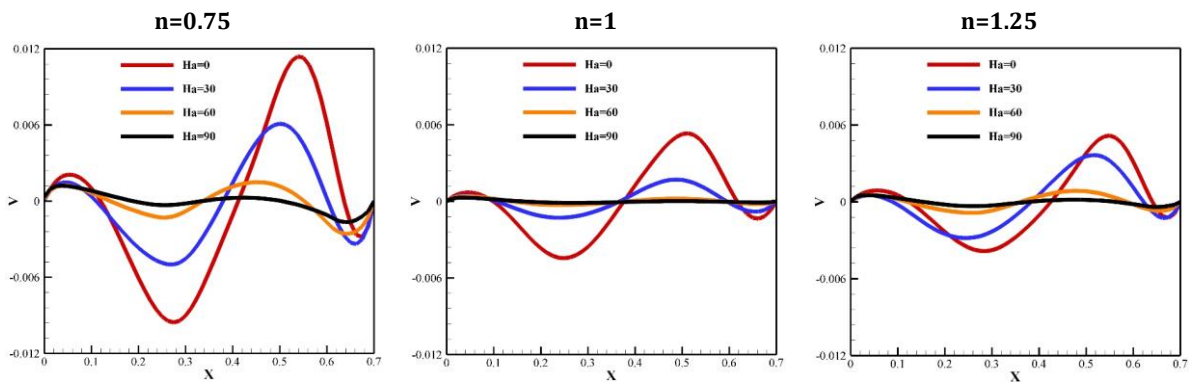


Figure 11. Vertical velocity due to variation of the *Ha* value and the *PLI* value at $Ra=10^5$

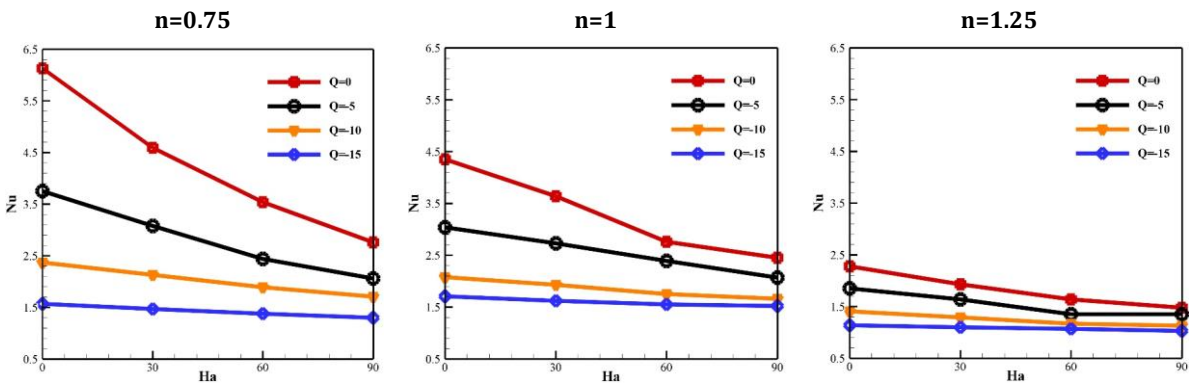


Figure 12 (a). The mean *Nu* value due to variation of the *Ha* value, the *PLI* value and heat absorption coefficient at $Ra=10^5$

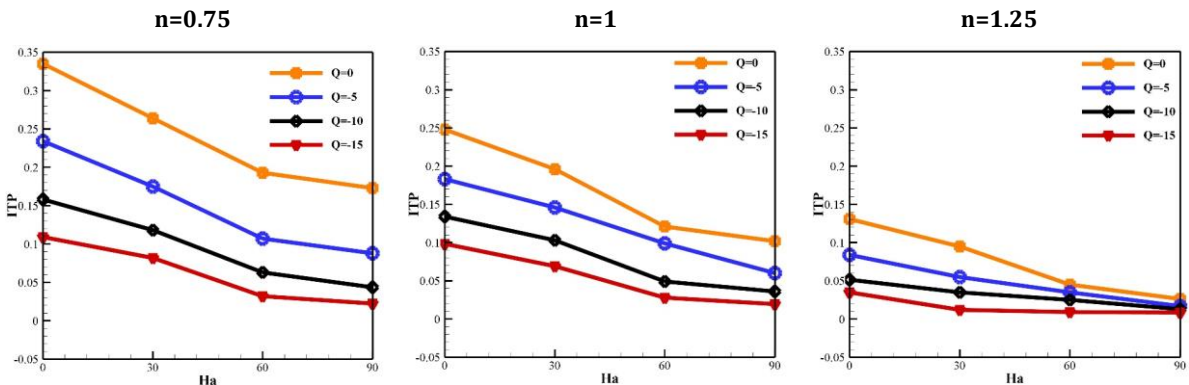


Figure 12 (b). The value of the *ITP* due to variation of the *Ha* value, the *PLI* value and heat absorption coefficient at $Ra=10^5$

Conclusions

In the discussions related to the equipment design in which the *HT* process is important, attaining optimal conditions has always been one of the challenges for scholars and designers. Although achieving the highest *HT* rate is very important in cooling parts that need to be cooled, equally important is the amount of the *PE* during the *HT* process. Analyzing the system thermal performance makes it possible to estimate the optimal conditions (the highest amount of *HT* at the lowest amount of *PE*). The need to cool hot parts in limited and unwanted spaces in industries such as electronics, nuclear, food production, etc. has motivated this numerical simulation via *LBM*. For this target, the cooling of two hot half-cylinders with variable positions in the space limited to an inclined triangular enclosure containing non-Newtonian nanofluid subjected to heat absorption and magnetic field (non-uniform and uniform) during the *FCHT* was studied. Some key outcomes are listed below:

- 1- Although the introduction of Lorentz resisting force into the fluid flow through the application of *MF* leads to a decrease in *PE*, it greatly reduces the average *Nu* value and the *ITP*. In order to decline the negative effect of applying *MF* on the system performance index, it is indispensable to exert *MF* non-uniformly, especially in the form of *MFM2*. Applying *MFM2* at the highest *Ha* value improves performance index and the average *Nu* value by about 40% and 49%, respectively. At low values of the *Ha* and the *Ra*, the change in the form of imposing the *MF* is not effective.
- 2- The cooling performance of the system is highly dependent on the arrangement of the hot objects on the walls. By reducing the distance between the hot objects and the cold wall, the average *Nu* value and the *ITP* value enhance. However, the highest effects of thermal convection can be observed for placing hot bodies in the central part of the adiabatic walls. For this reason, the greatest impact of the *MF* is reported in situation 2.
- 3- By rotating the chamber in different angles, the thermal characteristics of the system are completely changed in such a way that for the angles of 180 and 225 degrees, there is the lowest mean *Nu* value, the lowest the *ITP* value, the lowest *MF* effect, and the lowest convection effects. The change in the thermal characteristics for different inclination angles of the chamber is minimal for situation 1. Although for $\lambda=0$ and $\lambda=45^\circ$, an increase in *MF* leads to a decrease in the *ITP*, but for $\lambda=180^\circ$ in situation 3 and for $\lambda=225^\circ$ in situation 2 and situation 3, an increase in the value of the *ITP* can be seen as the value of the *Ha* enhances.
- 4- The presence of heat absorption disrupts the cooling process. The lowest value of the average *Nu* value and the *ITP* value is for the highest value of the heat absorption coefficient. The greatest impact of enhancing the heat absorption coefficient can be achieved by reducing the buoyancy force power so that in $Ra=10^4$, thermal conduction is the main mechanism of *HT* (*HT* at the molecular level). As the *PLI* enhances, the influence of heat absorption becomes weaker.

Nomenclature

B	Magnetic field power
c_i	Velocity of particles in different directions of the grid
f	Distribution function for flow field modeling
g	Acceleration of gravity
h	Distribution function for temperature field modeling
Ha	The Hartmann number
ITP	Index of thermal performance
n	Fluid behavioral index
MFM	Form of applied magnetic field
Nu	The mean Nusselt number
\tilde{Q}	Heat absorption parameter
Q	Heat absorption index
Ra	The Rayleigh number
S	Total entropy
\mathbf{u} (u, v)	Velocity in x and y directions
\mathbf{x} (x,y)	Geometry coordinate
θ	Dimensionless temperature
μ	Dynamic viscosity
ν	Kinematic viscosity
τ	Stress tensor
φ	The percentage of nanoparticles
Ψ	Stream function
λ	Angle of cavity placement

Conflicts of Interest

The author declares that there is no conflict of interest regarding the publication of this article.

References

- [1] Sajjadi, H., Nabavi, S.N., Atashafrooz, M. and Amiri Delouei, A., 2023. Optimization of Heating and Cooling System Locations by Taguchi's Method to

- Maximize or Minimize the Natural Convection Heat Transfer Rate in a Room. *Iranian Journal of Science and Technology, Transactions of Mechanical Engineering*, pp.1-16.
- [2] Mohebbi, R., Abbaszade, A., Varzandeh, M. and Ma, Y., 2021. Natural Convection Heat Transfer of Ag-MgO/Water Micropolar Hybrid Nanofluid inside an F-shaped Cavity Equipped by Hot Obstacle. *Journal of Heat and Mass Transfer Research*, 8(2), pp.139-150.
- [3] Omidpanah, M., Mirjalily, S.A.A., Kargarsharifabad, H. and Shoeibi, S., 2021. Numerical simulation of combined transient natural convection and volumetric radiation inside hollow bricks. *Journal of Heat and Mass Transfer Research*, 8(2), pp.151-162.
- [4] Ma, Y., Shahsavari, A., Moradi, I., Rostami, S., Moradikazerouni, A., Yarmand, H. and Zulkifli, N.W.B.M., 2021. Using finite volume method for simulating the natural convective heat transfer of nano-fluid flow inside an inclined enclosure with conductive walls in the presence of a constant temperature heat source. *Physica A: Statistical Mechanics and its Applications*, 580, p.123035.
- [5] Kolsi, L., Hussain, S., Ghachem, K., Jamal, M. and Maatki, C., 2022. Double diffusive natural convection in a square cavity filled with a porous media and a power law fluid separated by a wavy interface. *Mathematics*, 10(7), p.1060.
- [6] Pasha, A.A., Alam, M.M., Tayebi, T., Kasim, S., Dogonchi, A.S., Irshad, K., Chamkha, A.J., Khan, J. and Galal, A.M., 2023. Heat transfer and irreversibility evaluation of non-Newtonian nanofluid density-driven convection within a hexagonal-shaped domain influenced by an inclined magnetic field. *Case Studies in Thermal Engineering*, 41, p.102588.
- [7] Meenakshi, V., 2021. Dufour and Soret Effect on Unsteady MHD Free Convection and Mass Transfer Flow Past an Impulsively Started Vertical Porous Plate Considering with Heat Generation. *Journal of Heat and Mass Transfer Research*, 8(2), pp.257-266.
- [8] Nemati, M. and Sefid, M., 2023. The possibility of availing active and passive methods to achieve a flow with desirable characteristics via using the lattice Boltzmann method. *Engineering Analysis with Boundary Elements*, 146, pp.786-807.
- [9] Landl, M., Prieler, R., Monaco, E. and Hochenauer, C., 2023. Numerical Investigation of Conjugate Heat Transfer and Natural Convection Using the Lattice-Boltzmann Method for Realistic Thermophysical Properties. *Fluids*, 8(5), p.144.
- [10] Bai, J., Hu, X., Tao, Y.H. and Ji, W.H., 2022. Investigation of non-Newtonian power-law free convection affected by a magnetic field in an inclined quarter-circle chamber containing the lozenge-shaped obstacle via MRT-LBM of first and second laws of thermodynamics. *Engineering Analysis with Boundary Elements*, 145, pp.335-351.
- [11] Zaim, A., Aissa, A., Mebarek-Oudina, F., Mahanthesh, B., Lorenzini, G., Sahnoun, M. and El Ganaoui, M., 2020. Galerkin finite element analysis of magneto-hydrodynamic natural convection of Cu-water nanofluid in a baffled U-shaped enclosure. *Propulsion and Power Research*, 9(4), pp.383-393.
- [12] Sheikholeslami, M., 2019. Numerical approach for MHD Al₂O₃-water nanofluid transportation inside a permeable medium using innovative computer method. *Computer Methods in Applied Mechanics and Engineering*, 344, pp.306-318.
- [13] Baniamerian, Z. and Karimi, A., 2022. Multi Objective Optimization of Shell & Tube Heat Exchanger by Genetic, Particle Swarm and Jaya Optimization algorithms; Assessment of Nanofluids as the Coolant. *Journal of Heat and Mass Transfer Research*, 9(1), pp.1-16.
- [14] Atashafrooz, M., Sajjadi, H. and Delouei, A.A., 2023. Simulation of combined convective-radiative heat transfer of hybrid nanofluid flow inside an open trapezoidal enclosure considering the magnetic force impacts. *Journal of Magnetism and Magnetic Materials*, 567, p.170354.
- [15] Sheikholeslami, M., 2018. Magnetic source impact on nanofluid heat transfer using CVFEM. *Neural Computing and Applications*, 30, pp.1055-1064.
- [16] Nemati, M., Sefid, M., Karimpour, A. and Chamkha, A.J., 2023. Computational thermal performance analysis by LBM for cooling a hot oval object via magnetohydrodynamics non-Newtonian free convection by using magneto-ferrofluid. *Journal of Magnetism and Magnetic Materials*, 577, p.170797.
- [17] Atashafrooz, M., 2020. Influence of radiative heat transfer on the thermal characteristics of nanofluid flow over an inclined step in the presence of an axial magnetic field. *Journal of Thermal Analysis and Calorimetry*, 139(5), pp.3345-3360.
- [18] Sheikholeslami, M., 2019. New computational approach for exergy and entropy analysis of nanofluid under the impact of Lorentz force through a porous media. *Computer Methods in Applied Mechanics and Engineering*, 344, pp.319-333.
- [19] Rajkumar, D., Subramanyam Reddy, A. and Chamkha, A.J., 2022. Entropy generation of magnetohydrodynamic pulsating flow of micropolar nanofluid in a porous channel through Cattaneo-Christov heat flux model with Brownian motion, thermophoresis and heat source/sink. *Waves in Random and Complex Media*, pp.1-26.
- [20] Zhao, T.H., Khan, M.I. and Chu, Y.M., 2023. Artificial neural networking (ANN) analysis for heat and entropy generation in flow of non-Newtonian fluid between two rotating disks. *Mathematical Methods in the Applied Sciences*, 46(3), pp.3012-3030.
- [21] Ashorynejad, H.R., Javaherdeh, K., Sheikholeslami, M. and Ganji, D.D., 2014. Investigation of the heat transfer of a non-Newtonian fluid flow in an axisymmetric channel with porous wall using Parameterized Perturbation Method (PPM). *Journal of the Franklin Institute*, 351(2), pp.701-712.
- [22] Shahzad, H., Wang, X., Ghaffari, A., Iqbal, K., Hafeez, M.B., Krawczuk, M. and Wojnicz, W., 2022. Fluid structure interaction study of non-Newtonian Casson fluid in a bifurcated channel

- having stenosis with elastic walls. *Scientific Reports*, 12(1), p.12219.
- [23] Kumar, M.A., Reddy, Y.D., Goud, B.S. and Rao, V.S., 2022. An impact on non-Newtonian free convective MHD Casson fluid flow past a vertical porous plate in the existence of Soret, Dufour, and chemical reaction. *International Journal of Ambient Energy*, 43(1), pp.7410-7418.
- [24] Nazir, U. and Mukdasai, K., 2023. Combine influence of Hall effects and viscous dissipation on the motion of ethylene glycol conveying alumina, silica and titania nanoparticles using the non-Newtonian Casson model. *AIMS Maths*, 8(2), pp.4682-99.
- [25] Nemati, M., Sefid, M. and J Chamkha, A., 2022. Heat transfer and entropy generation of power-law fluids natural convection inside triangular cavity; The effect of angle and type of magnetic field applied. *Energy Equipment and Systems*, 10(4), pp.327-352.
- [26] Nemati, M., Sefid, M. and Rahmati, A., 2021. Analysis of the effect of periodic magnetic field, heat absorption/generation and aspect ratio of the enclosure on non-Newtonian natural convection. *Journal of Heat and Mass Transfer Research*, 8(2), pp.187-203.
- [27] Shehzad, N., Zeeshan, A., Shakeel, M., Ellahi, R. and Sait, S.M., 2022. Effects of magnetohydrodynamics flow on multilayer coatings of Newtonian and non-Newtonian fluids through porous inclined rotating channel. *Coatings*, 12(4), p.430.
- [28] Nemati, M. and Sefid, M., 2022. Using active/passive methods to control of MHD conjugate heat transfer of power-law fluids: a numerical entropy analysis by LBM. *International Journal of Energy and Environmental Engineering*, pp.1-23.
- [29] Sun, C., Zhang, Y., Farahani, S.D., Hu, C., Nemati, M. and Sajadi, S.M., 2022. Analysis of power-law natural conjugate heat transfer under the effect of magnetic field and heat absorption/production based on the first and second laws of thermodynamics for the entropy via lattice Boltzmann method. *Engineering Analysis with Boundary Elements*, 144, pp.165-184.
- [30] Shah, I.A., Bilal, S., Akgül, A., Omri, M., Bouslimi, J. and Khan, N.Z., 2022. Significance of cold cylinder in heat control in power law fluid enclosed in isosceles triangular cavity generated by natural convection: A computational approach. *Alexandria Engineering Journal*, 61(9), pp.7277-7290.
- [31] Sajjadi, H., Amiri Delouei, A. and Atashafrooz, M., 2023. Effect of magnetic field on particle deposition in a modeled room. *Particulate Science and Technology*, 41(3), pp.361-370.
- [32] Atashafrooz, M., Sajjadi, H. and Delouei, A.A., 2020. Interacting influences of Lorentz force and bleeding on the hydrothermal behaviors of nanofluid flow in a trapezoidal recess with the second law of thermodynamics analysis. *International Communications in Heat and Mass Transfer*, 110, p.104411.
- [33] Atashafrooz, M., 2019. The effects of buoyancy force on mixed convection heat transfer of MHD nanofluid flow and entropy generation in an inclined duct with separation considering Brownian motion effects. *Journal of Thermal Analysis and Calorimetry*, 138(5), pp.3109-3126.
- [34] Hameed, N., Noeiaghdam, S., Khan, W., Pimpunchat, B., Fernandez-Gamiz, U., Khan, M.S. and Rehman, A., 2022. Analytical analysis of the magnetic field, heat generation and absorption, viscous dissipation on couple stress casson hybrid nano fluid over a nonlinear stretching surface. *Results in Engineering*, 16, p.100601.
- [35] Nemati, M. and Farahani, S.D., 2023. Using lattice Boltzmann method to control entropy generation during conjugate heat transfer of power-law liquids with magnetic field and heat absorption/production. *Computational Particle Mechanics*, 10(3), pp.331-354.
- [36] Majeed, A., Zeeshan, A., Noori, F.M. and Masud, U., 2019. Influence of rotating magnetic field on Maxwell saturated ferrofluid flow over a heated stretching sheet with heat generation/absorption. *Mechanics & Industry*, 20(5), p.502.
- [37] Nazeer, M., Ali, N. and Javed, T., 2018. Natural convection flow of micropolar fluid inside a porous square conduit: effects of magnetic field, heat generation/absorption, and thermal radiation. *Journal of Porous Media*, 21(10).
- [38] Selimefendigil, F. and Özttop, H.F., 2019. MHD mixed convection of nanofluid in a flexible walled inclined lid-driven L-shaped cavity under the effect of internal heat generation. *Physica A: Statistical Mechanics and its Applications*, 534, p.122144.
- [39] Afsana, S., Molla, M.M., Nag, P., Saha, L.K. and Siddiqa, S., 2021. MHD natural convection and entropy generation of non-Newtonian ferrofluid in a wavy enclosure. *International Journal of Mechanical Sciences*, 198, p.106350.
- [40] Hussain, S., Özttop, H.F., Mehmood, K. and Abu-Hamdeh, N., 2018. Effects of inclined magnetic field on mixed convection in a nanofluid filled double lid-driven cavity with volumetric heat generation or absorption using finite element method. *Chinese journal of physics*, 56(2), pp.484-501.
- [41] Sajedi, M., Safavinejad, A. and Atashafrooz, M., 2023. Numerical analysis of entropy generation in a two-dimensional porous heat recovery system. *Journal of Porous Media*, 26(2).
- [42] Cao, Y., Mansir, I.B., Singh, P.K., Ali, H.E., Abed, A.M., El-Refaey, A.M., Aly, A.A., Nguyen, D.T., Wae-hayee, M. and Tran, D.C., 2023. Heat transfer analysis on ferrofluid natural convection system with magnetic field. *Ain Shams Engineering Journal*, 14(9), p.102122.
- [43] Tabarhoseini, S.M. and Sheikholeslami, M., 2022. Entropy generation and thermal analysis of nanofluid flow inside the evacuated tube solar collector. *Scientific Reports*, 12(1), p.1380.
- [44] Pordanjani, A.H., Aghakhani, S., Alnaqi, A.A. and Afrand, M., 2019. Effect of alumina nano-powder on the convection and the entropy generation of water inside an inclined square cavity subjected to a magnetic field: uniform and non-uniform

- temperature boundary conditions. *International Journal of Mechanical Sciences*, 152, pp.99-117.
- [45] Iftikhar, B., Siddiqui, M.A. and Javed, T., 2023. Dynamics of magnetohydrodynamic and ferrohydrodynamic natural convection flow of ferrofluid inside an enclosure under non-uniform magnetic field. *Alexandria Engineering Journal*, 66, pp.523-536.
- [46] Hossain, A., Nag, P. and Molla, M.M., 2022. Mesoscopic simulation of MHD mixed convection of non-newtonian ferrofluids with a non-uniformly heated plate in an enclosure. *Physica Scripta*, 98(1), p.015008.
- [47] Jiang, X., Hatami, M., Abderrahmane, A., Younis, O., Makhdoum, B.M. and Guedri, K., 2023. Mixed convection heat transfer and entropy generation of MHD hybrid nanofluid in a cubic porous cavity with wavy wall and rotating cylinders. *Applied Thermal Engineering*, 226, p.120302.
- [48] Daneshvar Garmroodi, M.R., Ahmadpour, A., Hajmohammadi, M.R. and Gholamrezaie, S., 2020. Natural convection of a non-Newtonian ferrofluid in a porous elliptical enclosure in the presence of a non-uniform magnetic field. *Journal of Thermal Analysis and Calorimetry*, 141, pp.2127-2143.
- [49] Kandelousi, M.S. and Ellahi, R., 2015. Simulation of ferrofluid flow for magnetic drug targeting using the lattice Boltzmann method. *Zeitschrift für Naturforschung A*, 70(2), pp.115-124.
- [50] Banik, S., Mirja, A.S., Biswas, N. and Ganguly, R., 2022. Entropy analysis during heat dissipation via thermomagnetic convection in a ferrofluid-filled enclosure. *International Communications in Heat and Mass Transfer*, 138, p.106323.
- [51] Abro, K.A., Khan, I. and Gomez-Aguilar, J.F., 2021. Heat transfer in magnetohydrodynamic free convection flow of generalized ferrofluid with magnetite nanoparticles. *Journal of Thermal Analysis and Calorimetry*, 143, pp.3633-3642.
- [52] Khoshtarash, H., Siavashi, M., Ramezanpour, M. and Blunt, M.J., 2023. Pore-scale analysis of two-phase nanofluid flow and heat transfer in open-cell metal foams considering Brownian motion. *Applied Thermal Engineering*, 221, p.119847.
- [53] Shamshuddin, M.D., Mabood, F. and Bég, O.A., 2022. Thermomagnetic reactive ethylene glycol-metallic nanofluid transport from a convectively heated porous surface with Ohmic dissipation, heat source, thermophoresis and Brownian motion effects. *International Journal of Modelling and Simulation*, 42(5), pp.782-796.
- [54] Upreti, H., Pandey, A.K., Uddin, Z. and Kumar, M., 2022. Thermophoresis and Brownian motion effects on 3D flow of Casson nanofluid consisting microorganisms over a Riga plate using PSO: A numerical study. *Chinese Journal of Physics*, 78, pp.234-270.
- [55] Nemati, M. and Chamkha, A.J., 2023. Examination of effective strategies on changing the amount of heat transfer and entropy during non-Newtonian magneto-nanofluid mixed convection inside a semi-ellipsoidal cavity. *Journal of Magnetism and Magnetic Materials*, 578, p.170652.
- [56] Nazari, M., Mohebbi, R. and Kayhani, M.H., 2014. Power-law fluid flow and heat transfer in a channel with a built-in porous square cylinder: Lattice Boltzmann simulation. *Journal of non-Newtonian fluid mechanics*, 204, pp.38-49.
- [57] Kebriti, S. and Moqtaderi, H., 2021. Numerical simulation of convective non-Newtonian power-law solid-liquid phase change using the lattice Boltzmann method. *International Journal of Thermal Sciences*, 159, p.106574.
- [58] Shahriari, A., Ashorynejad, H.R. and Pop, I., 2019. Entropy generation of MHD nanofluid inside an inclined wavy cavity by lattice Boltzmann method. *Journal of Thermal Analysis and Calorimetry*, 135, pp.283-303.
- [59] Wang, L., Zhao, Y., Yang, X., Shi, B. and Chai, Z., 2019. A lattice Boltzmann analysis of the conjugate natural convection in a square enclosure with a circular cylinder. *Applied Mathematical Modelling*, 71, pp.31-44.
- [60] Khan, F., Xiao-Dong, Y., Aamir, N., Saeed, T. and Ibrahim, M., 2023. The effect of radiation on entropy and heat transfer of MHD nanofluids inside a quarter circular enclosure with a changing L-shaped source: lattice Boltzmann methods. *Chemical Engineering Communications*, 210(5), pp.740-755.
- [61] Farkach, Y., Derfoufi, S., Ahachad, M., Bahraoui, F. and Mahdaoui, M., 2022. Numerical investigation of natural convection in concentric cylinder partially heated based on MRT-lattice Boltzmann method. *International Communications in Heat and Mass Transfer*, 132, p.105856.
- [62] Alqahtani, A.M., Sajadi, S.M., Al Hazmi, S.E., Alsenani, T.R., Alqurashi, R.S. and El Bouz, M.A., 2023. Entropy generation and mixed convection in an enclosure with five baffles exposed to a uniform magnetic field with volumetric radiation for the solar collectors via lattice Boltzmann method. *Engineering Analysis with Boundary Elements*, 150, pp.285-297.
- [63] Aljaloud, A.S.M., 2023. Hybrid nanofluid mixed convection in a cavity under the impact of the magnetic field by lattice Boltzmann method: Effects of barrier temperature on heat transfer and entropy. *Engineering Analysis with Boundary Elements*, 147, pp.276-291.
- [64] Moradi, I. and D'Orazio, A., 2023. Lattice Boltzmann Method Pore-scale simulation of fluid flow and heat transfer in porous media: Effect of size and arrangement of obstacles into a channel. *Engineering Analysis with Boundary Elements*, 152, pp.83-103.
- [65] Kashyap, D. and Dass, A.K., 2018. Two-phase lattice Boltzmann simulation of natural convection in a Cu-water nanofluid-filled porous cavity: Effects of thermal boundary conditions on heat transfer and entropy generation. *Advanced Powder Technology*, 29(11), pp.2707-2724.
- [66] Himika, T.A., Hassan, S., Hasan, M.F. and Molla, M.M., 2020. Lattice Boltzmann Simulation of MHD Rayleigh-Bénard Convection in Porous Media. *Arabian Journal for Science and Engineering*, 45(11), pp.9527-9547.
- [67] Ferhi, M., Djebali, R., Mebarek-Oudina, F., Abu-Hamdeh, N.H. and Abboudi, S., 2022. Magnetohydrodynamic free convection through entropy generation scrutiny of eco-friendly nanoliquid in a divided L-shaped heat exchanger

- with lattice Boltzmann method simulation. *Journal of Nanofluids*, 11(1), pp.99-112.
- [68] Mohebbi, R., Izadi, M., Sajjadi, H., Delouei, A.A. and Sheremet, M.A., 2019. Examining of nanofluid natural convection heat transfer in a Γ -shaped enclosure including a rectangular hot obstacle using the lattice Boltzmann method. *Physica A: Statistical Mechanics and its Applications*, 526, p.120831.
- [69] Rezaie, M.R. and Norouzi, M., 2018. Numerical investigation of MHD flow of non-Newtonian fluid over confined circular cylinder: a lattice Boltzmann approach. *Journal of the Brazilian Society of Mechanical Sciences and Engineering*, 40, pp.1-10.
- [70] Nemati, M., Sefid, M., Jahromi, B. and Jahangiri, R., 2022. The effect of magnetic field and nanoparticle shape on heat transfer in an inclined cavity with uniform heat generation/absorption. *Journal of Computational Methods in Engineering*, 40(2), pp.109-126.
- [71] Filippova, O. and Hänel, D., 1998. Grid refinement for lattice-BGK models. *Journal of Computational physics*, 147(1), pp.219-228.
- [72] Ding, L., Shi, W., Luo, H. and Zheng, H., 2009. Investigation of incompressible flow within $\frac{1}{2}$ circular cavity using lattice Boltzmann method. *International journal for numerical methods in fluids*, 60(8), pp.919-936.
- [73] Ashorynejad, H.R. and Shahriari, A., 2018. MHD natural convection of hybrid nanofluid in an open wavy cavity. *Results in Physics*, 9, pp.440-455.